Toward Application of Limit Cycle Based Walking to Humanoid Robots

Master Thesis Presented to

the Graduate School of Engineering,

Musashi Institute of Technology

in Partial Fulfillment of the Requirements

for the Degree of Master of Engineering Course

0881221 Yuzuru Harada
Advisor: Prof. Dragomir N. Nenchev
Dr. Daisuke Sato

January, 29th 2010

Contents

List of Figures

List of Tables

Chapter 1

Introduction

1.1 Background

At present, humanoid robots are studied by many manufacturers and research institutes. Humanoid robots are the ultimate personification machines, therefore they are able to become the labor power for unattractive and hard work. In addition, they in a way are an advertising pillar of advanced technology for manufacturers and research institutes. At present, most humanoid robots comprise minimal capabilities, for example of biped walking and balance keeping. The field of application of humanoid robots is mainly for education, research or entertainment. Hence, progressive intelligent technology has to be implemented and evaluated in the years-ahead [1]. Humanoid robots have naturally advantageous interfaces. In a human dwelling environment, bipeds with small turning circle can be appreciated as a locomotion morphology. In addition, biped walking can be performed on irregular ground, with discontinuous characteristics like steps or ditches. However, it is difficult to generate and control biped walking, with regard to stability and efficiency. Therefore, the field of biped control should be studied more and perfected further.

1.2 ZMP Based Walking Control

One of the most advanced humanoid robots is ASIMO of Honda, it can achieve high-quality biped walking. There are three main points of Honda's biped walking technologies:

1. development of hardware based on analysis of humans,
2. adoption of flexible gum sole,
3. stabilization of posture with Zero Moment Point (ZMP) control.

Briefly, the keys to success in the development are accumulated improvements of the hardware and control based on a stability indicator called ZMP. Biped walking control based on ZMP has been studied by many researchers, and has reached almost the stage of completion.

The basis of ZMP based walking control method is correcting of the difference between a reference ZMP trajectory and the actual ZMP derived from robot sensors during walking. Figure 1.1 shows the basic control mechanism based on the relation between ZMP and center of mass (CoM). Both Fig. 1.1 (a) and (b) indicate this relation. The relation between ZMP and CoM of these models is written as followings:

$$p = r_{Cx} - \frac{r_{Cz}}{g}\ddot{r}_{Cx}, \tag{1.1}$$

where r_C denotes CoM position, p denotes ZMP and g denotes gravity acceleration. This equation is the fundament for ZMP based walking control.

Kajita's Linear Inverted Pendulum Mode [2] is known as an useful control method based on ZMP with regard to the dynamics of humanoid robots represented as an inverted pendulum that maintains the height of the center of mass (CoM). This control method actualizes real-time performance and the robust stability of walking by a simple mechanism. Therefore, it combines practicality and expandability, when on uneven ground. Problems of

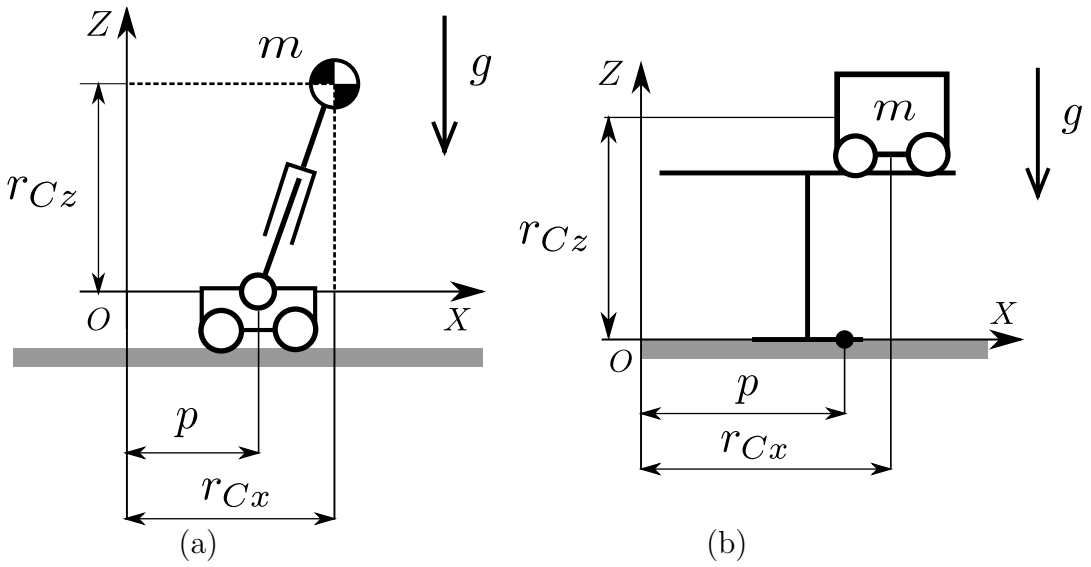

Fig. 1.1: ZMP based control basics: (a) the case of ZMP input, (b) the case of CoM input.

this control method are energy efficiency and naturalness. In addition, this sort of control method depends on the inverse kinematics to manipulate the ZMP or the CoM [3], therefore, it has the inherent problem of singularity. Hence, it is impossible for biped robots to take a stance with straight-knees, therefore, they are controlled with bended knees. This problem concerns energy efficiency because a bended knee stance consumes more energy than a straight knee one [4]. Besides, generally, ZMP based control uses dynamics of the coarse model as shown in Fig. 1.1. Therefore, this control cannot use the dynamics features of robots entirely. We think that using the model dynamics is very important for generating natural and efficient walking.

The central problem of biped locomotion has shifted recently to how to create a nice-looking and effective walking gait. However, traditional biped control methods cannot solve these problems, because they are based on a simplification of robots dynamics. On the other hand, many studies have

been reported so far on the gait optimization problem w.r.t.[1] the system's energy consumption. Unfortunately, definitions and opinions on optimality are quite different. An unified concept hasn't been established yet since there aren't any models which can exhibit an optimal gait. Consequently, it is necessary to set a new unified paradigm of gait optimization. As a possible paradigm, we adopt a walking pattern called "Limit Cycle Walking", which is high-performance walking pattern from the point of view of naturalness and energy efficiency.

1.3 Passive Dynamic Walking

Another prospective method for walking pattern generation is the so-called "Passive Dynamic Walking (PDW)." PDW is one type of "Limit Cycle Walking" [5]. In that reference, Limit Cycle Walking was defined as "a nominally periodic sequence of steps that is stable as a whole, but not locally stable at any instant time."[2]

PDW has attracted attention as a suitable method to obtain a highly-efficient walking pattern [6]. PDW is realized on a shallow slope without active control or energy input. The mechanism of PDW is based on a condition of equilibrium between recovery of mechanical energy while walking and energy dissipation by a collision of a tip of the swing leg and floor. Consequently, a stable walking pattern is generated by dynamic interaction between the biped model and the environment. Especially, such walking pattern contains an important feature: there is a stable limit cycle.

[1] with respect to

[2] Stable oscillation must be produced by nonlinear systems. There are nonlinear systems that can go into an oscillation of fixed amplitude and frequency, irrespective of the initial state. This type of oscillation is known as "limit cycle."

1.3.1 Energy efficiency

PDW can be regarded as an ultimate walking pattern generation method from the view point of energy efficiency because PDW doesn't need any energy input or any control torques.

Limit Cycle Walkers use generally less energy than other existing biped robots. This is proven with the help of the energetic cost of transport ε [7]:

$$\varepsilon = \frac{P}{mgv}, \tag{1.2}$$

where P is the power which is consumed while walking, m is the total mass of the robot, g is the gravity acceleration, v is the velocity of transport. According to Table 1.1, except Delft University of Technogy's Denise, which is about an order of magnitude less efficient than Honda's ASIMO, the other Limit Cycle Walkers are more efficient. Cornell's powered biped especially shows the same performance as that of a human walking. As time advances, biped walking will be developed as more efficient than human walking.

Table 1.1: The ε comparison with several walkers.

Walking Object	ε
Passive Dynamic Walkers	0.0
Human	0.2
Cornell's powered biped	0.2
Honda's ASIMO	3.2
T.U. Delft's Denise	5.3

1.4 Issues Related to Passive Dynamic Walking

A lot of researchers have studied walking patterns based on the PDW concept [8], [9]. However, all of the PDW based walking patterns have a stability

problem. The stability of PDW depends on the system parameters and the initial conditions. So far, no explicit relation between initial conditions and stability is known. Therefore, the conditions are usually set empirically. But this is feasible only for simple models in the plane.

McGeer modeled 3D PDW incorporating both roll and yaw rotation and found it to be unstable [10][3]. The reason is that roll-to-pitch or yaw-to-pitch coupling inhibits the generation of a stable limit cycle for pitch motion. Some solutions have been proposed for stabilizing 3D walking, e.g. a method for roll motion stabilization [12] and using a pelvic upper body as yaw and roll compensator [11]. Consequently, an important keyword for 3D Limit Cycle Walking is decoupling. In turn, it is also important to take advantage of the existing stable limit cycle of pitch motion.

On the other hand, our study is characterized by the following concepts:

- control method design with the help of numerical simulation;
- the biped model shouldn't have special mechanisms for a passive gait if possible.

Firstly, we want to study three-dimensional Limit Cycle Walking in an ideal environment, because, we want to solve the problem of lack of a limit cycle in three-dimensional PDW, by using the robot dynamics and the environment. Besides, we think that we may understand the mechanism of Limit Cycle Walking through deriving the equation of motion and collision. Secondly, humanoid robots are required to perform many kinds of tasks. Hence we think that versatility is important for humanoid robots. So, we must solve some problems with joint actuation, if possible.

[3] Definitions of the axes and the planes in this paper is described in Appendix A.

1.5 Aim of This Study

The aim of our study is to generate a highly-efficient walking pattern for humanoid robots based on limit cycle. However, the limit cycle based walking pattern has some inherent problems. For example, it is difficult to find a stable limit cycle; also, the generated walking pattern based on limit cycle isn't robust because there aren't any feedback components from a reference trajectory. Therefore, Limit Cycle Walking is limited to simple planar biped models. Especially, we have been focusing on how to extend such biped models. Consequently, the main point of this study is how to extend the control of a simple biped model to the 3D complex biped model based on the PDW concept.

1.6 Outline of This Thesis

Chapter 2 deals with a 2D biped model called "compass biped model" because it is known to have a stable walking pattern generation under the PDW mechanism.

In Chapter 3, we deal with various extended 2D biped models. Humanoid robots have many degrees of freedom (DOF). However, the compass biped model mentioned has only two DOF. Therefore, to apply the PDW based control to humanoid robots, we have to extend the biped model. In this chapter, we propose a walking pattern generator for extended models based on limit cycle of the simple biped model. We expect that this method will enable us to generate stable walking pattern of extended biped models more easily than ever before.

In Chapter 4, we focus on 3D limit cycle based walking. In the past, we proposed a walking pattern generator for the simplest 3D biped model by combination of decoupling control, energy feedback control and so on [13]. This chapter tries to extend the control for complex 3D biped models.

In Chapter 5, we conclude this thesis and present future tasks to apply our control to humanoid robots.

Chapter 2

Fundamentals of Passive Biped Walking

This chapter deals with the simple 2D biped model which is called "compass biped model". Limit Cycle Walking of a compass biped model is the basic of the biped walking based on the PDW concept, because the model can walk without mechanical gimmicks and any feedback controls. Therefore, it is important to understand the mechanism and property of the biped walking generation of a compass biped model to extend the limit cycle based control.

2.1 Compass Biped Model

This chapter deals with the 2D compass biped model in the sagittal plane as shown in Fig. 2.1. The physical parameters of the compass biped model are shown in Table 2.1. The model is composed of only two links. We assume that there are foot links whose thickness and mass are ignored. We also assume the support leg to be always fixed to the ground. The generalized coordinates of the model are the joint angles: $\boldsymbol{q} = \begin{bmatrix} q_1 & q_2 \end{bmatrix}^T$, while the generalized force vector is represented in terms of joint torque as $\boldsymbol{\tau} = \begin{bmatrix} \tau_1 & \tau_2 \end{bmatrix}^T$. The total

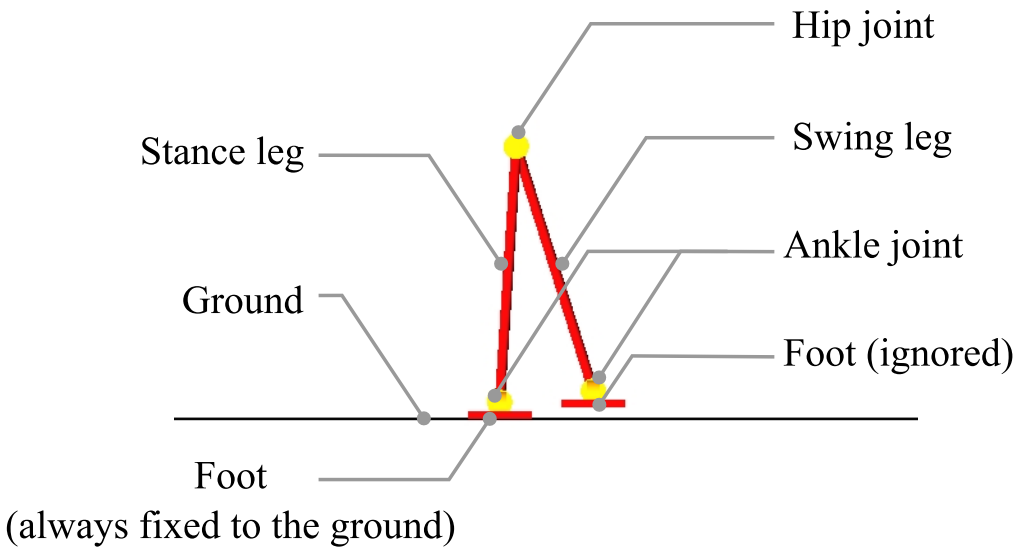

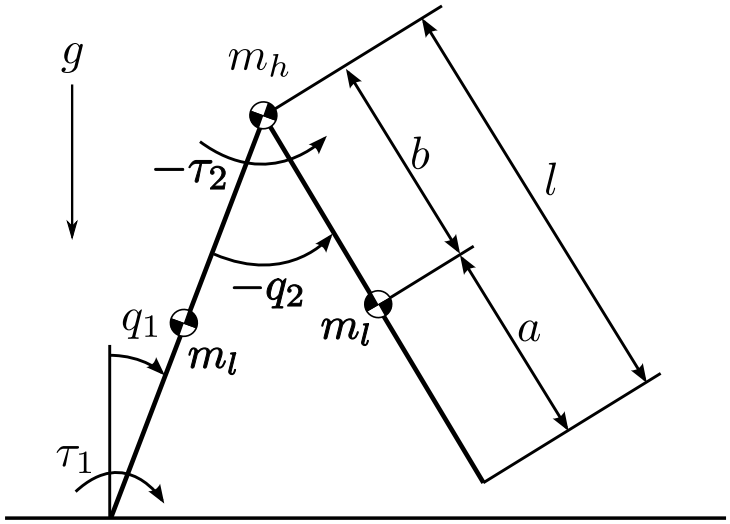

Fig. 2.1: Compass biped model.

Table 2.1: Physical parameters of the compass biped model.

Symbol	Parameter name	Value	
m_l	leg mass	5.0	kg
m_h	hip mass	10.0	kg
l	leg length	1.0	m
a	lower part of leg	0.5	m
b	upper part of leg	0.5	m

mass of the biped model is:

$$m_{tot} = 2m_l + m_h. \tag{2.1}$$

2.2 Passive Dynamic Walking Concept

PDW can be achieved on a shallow slope from a suitable initial state without any active control or any energy input as shown in Fig. 2.2. Note that the *foot-scuffing* during the single support phase is ignored. PDW system can be modeled as a hybrid system that includes a single support phase and a leg switch phase (Fig. 2.3). In the single support phase, the biped model performs walking motion. On the other hand, in the leg switch phase, the switching between the stance leg and the swing leg and the collision between the swing leg's end tip and ground are modeled. It is known that stable walking based on the PDW is periodic. Hence, we can say that initial state of the stable walking based on PDW concept is similar to the post collision state of the next step.

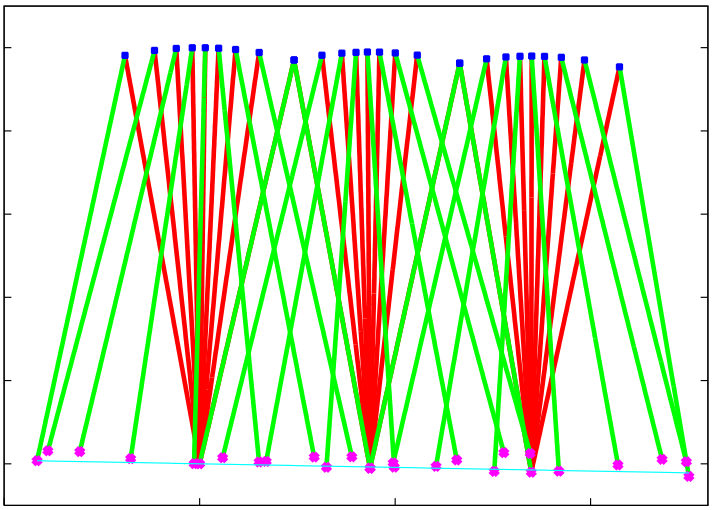

Fig. 2.2: Behavior of PDW.

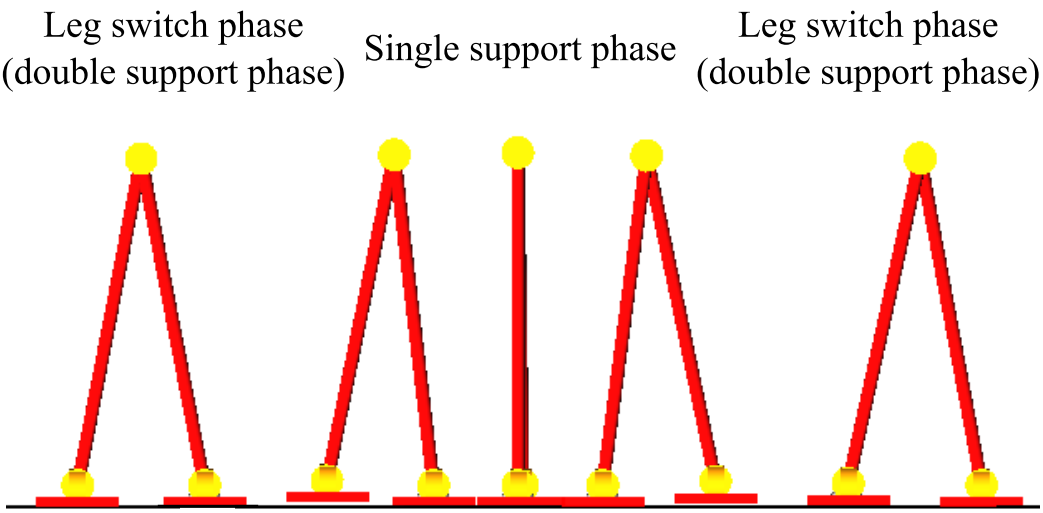

Fig. 2.3: Typical phases of biped walking.

2.2.1 Equation of motion

The equation of motion of the compass biped model during the single support phase is given as:

$$\boldsymbol{M}(\boldsymbol{q})\ddot{\boldsymbol{q}} + \boldsymbol{C}(\boldsymbol{q}, \dot{\boldsymbol{q}})\dot{\boldsymbol{q}} + \boldsymbol{g}(\boldsymbol{q}) = \boldsymbol{\tau} \tag{2.2}$$

where $\boldsymbol{M}(\boldsymbol{q}) \in \Re^{2\times 2}$ denotes the inertia matrix, $\boldsymbol{C}(\boldsymbol{q}, \dot{\boldsymbol{q}}) \in \Re^{2\times 2}$ is the Coriolis and centrifugal forces matrix, $\boldsymbol{g}(\boldsymbol{q}) \in \Re^2$ is the gravity term.

2.2.2 Equation of collision

The equation of impact dynamics models a collision between the swing leg's end-tip and the ground. We assume the collision is a completely inelastic one. Therefore, the collision equation is modeled after the principle of conservation of angular momentum:

$$\boldsymbol{Q}^-(\boldsymbol{q}^-)\dot{\boldsymbol{q}}^- = \boldsymbol{Q}^+(\boldsymbol{q}^+)\dot{\boldsymbol{q}}^+, \tag{2.3}$$

where superscripts $(\circ)^-$ and $(\circ)^+$ denote pre- and post- collision values, respectively, $\boldsymbol{q}^-, \boldsymbol{q}^+$ denote the expanded generalized coordinates for the equation of collision, $\boldsymbol{Q}^-(\boldsymbol{q}^-)\dot{\boldsymbol{q}}^-$ denotes the angular momentum at pre-collision and $\boldsymbol{Q}^+(\boldsymbol{q}^+)\dot{\boldsymbol{q}}^+$ denotes the angular momentum at post-collision, and $\boldsymbol{Q}^-(\boldsymbol{q}^-) \in \Re^{2\times 2}$ and $\boldsymbol{Q}^+(\boldsymbol{q}^+) \in \Re^{2\times 2}$ have the meaning of inertia matrices.

2.2.3 Analysis of PDW mechanism

As shown in Fig. 2.4 (left), the tangential element which is divided by the gravity acceleration g into a tangential component to the slope $g\sin\phi$ and a normal component $g\cos\phi$, acts as a driving force for the biped model. By regarding this as an active walking level as shown in Fig. 2.4 (right), the biped model seemed to be driven by the equivalent transformed torque in the virtual gravity field which magnitude is $g\cos\phi$. In this chapter, the transformed

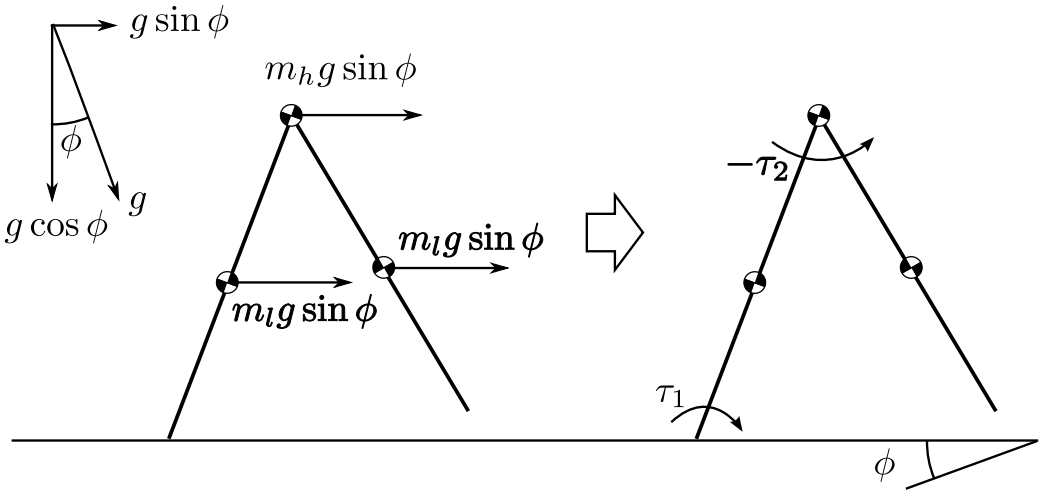

Fig. 2.4: PDW mechanism.

torque is called virtual torque. The virtual torque τ_ϕ is calculated as:

$$\boldsymbol{\tau}_\phi = \begin{bmatrix} m\boldsymbol{J}_{C1}^T \\ m\boldsymbol{J}_{C2}^T \\ m_h\boldsymbol{J}_{Ch}^T \end{bmatrix} \begin{bmatrix} g\sin\phi \\ 0 \end{bmatrix}, \tag{2.4}$$

$$= \boldsymbol{J}_C^T \boldsymbol{f}_g, \tag{2.5}$$

where $\boldsymbol{J}_{C(\circ)}$ denotes the center of mass (CoM) Jacobian matrix of each link, $\boldsymbol{J}_C$ is the Jacobian matrix for the total CoM and $\boldsymbol{f}_g$ is the control torque for driving the biped model. The mechanical energy E_ϕ in the virtual gravity field can be defined as:

$$E_\phi = \frac{1}{2}\dot{\boldsymbol{q}}^T \boldsymbol{M}\dot{\boldsymbol{q}} + P_\phi \tag{2.6}$$

where P_ϕ is the virtual potential energy based on the virtual gravity field.

Figure 2.5 shows numerical simulation results of PDW of the compass biped model with a shallow slope of angle $\phi = 0.017$ rad. From Fig. 2.5 (a), we can see that flat control torques are generated. Figure 2.5 (b) shows that the virtual mechanical energy is restored monotonically during the single

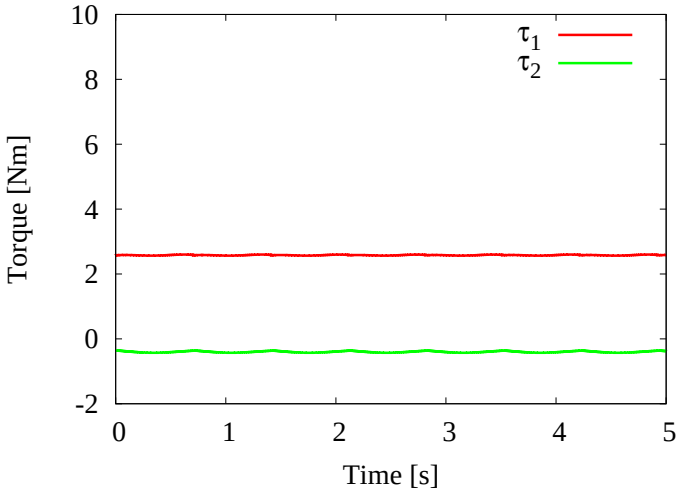

(a)

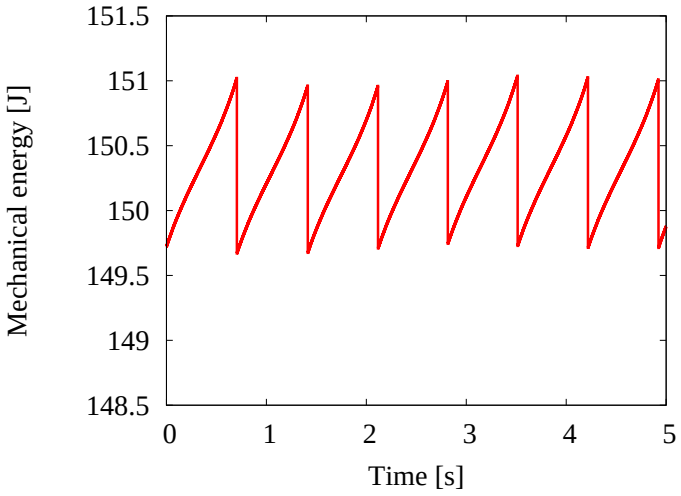

(b)

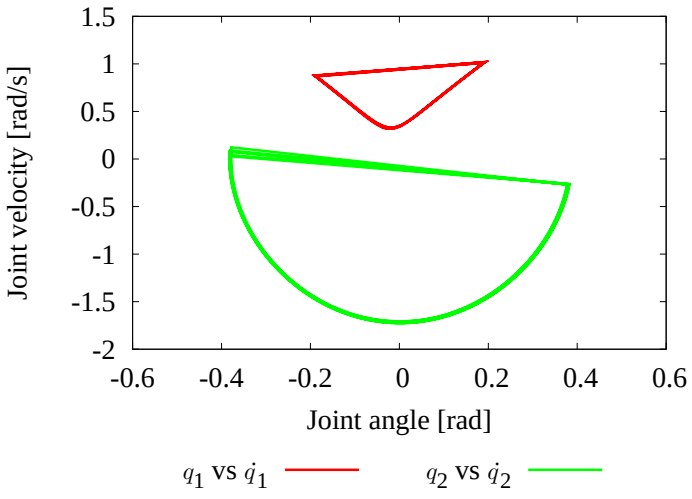

(c)

Fig. 2.5: Simulation results of PDW where $\phi = 0.017$ rad: (a) virtual control torque, (b) virtual mechanical energy, (c) phase portrait.

support phase by virtual control torques. From the phase portrait as shown in Fig. 2.5 (c), we can confirm that stable PDW is periodic.

2.3 Virtual Passive Dynamic Walking

Virtual Passive Dynamic Walking (VPDW) was proposed by Asano *et al.* [14]. This method is the most intuitive control method of imitating the mechanism of PDW. It uses a small artificial gravity called "virtual gravity" toward direction of movement. Active dynamic walking can be realized via equivalent torque transformation of the virtual gravity effect, as shown in Fig. 2.6. The

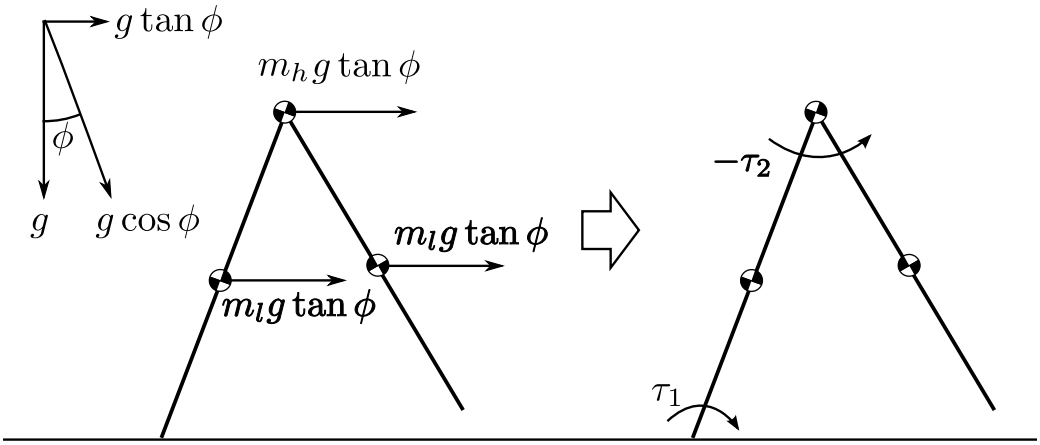

Fig. 2.6: Virtual Passive Dynamic Walking mechanism.

equivalent transformed torque is given by:

$$\boldsymbol{\tau} = \boldsymbol{J}_C^T \boldsymbol{f}_{vg}, \tag{2.7}$$

where $\boldsymbol{f}_{vg} = \begin{bmatrix} m_{tot} g \tan \phi & 0 \end{bmatrix}^T$ is the virtual gravity, ϕ is virtual slope angle.

Figure 2.7 shows the simulation results of VPDW. We can see that the shape of control torque and mechanical energy are quite similar to those of PDW (Fig. 2.5).

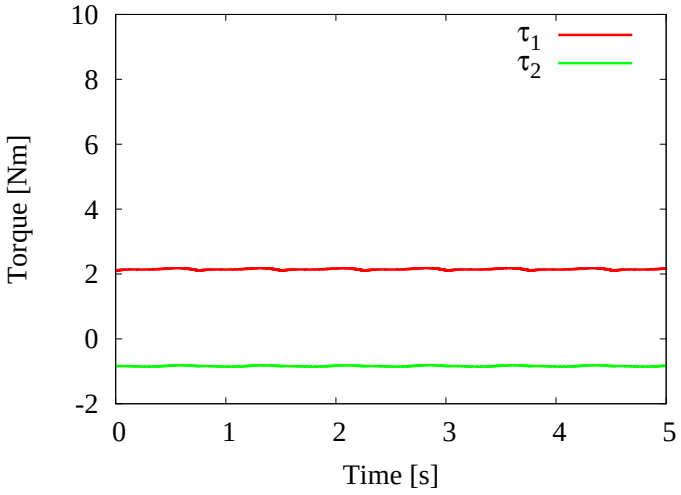

(a)

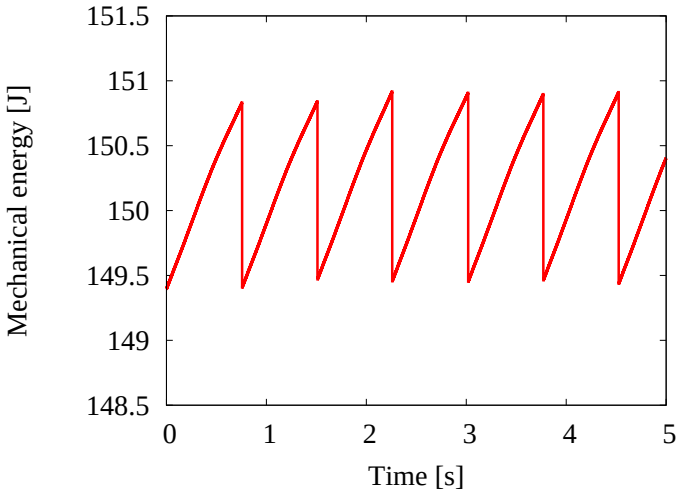

(b)

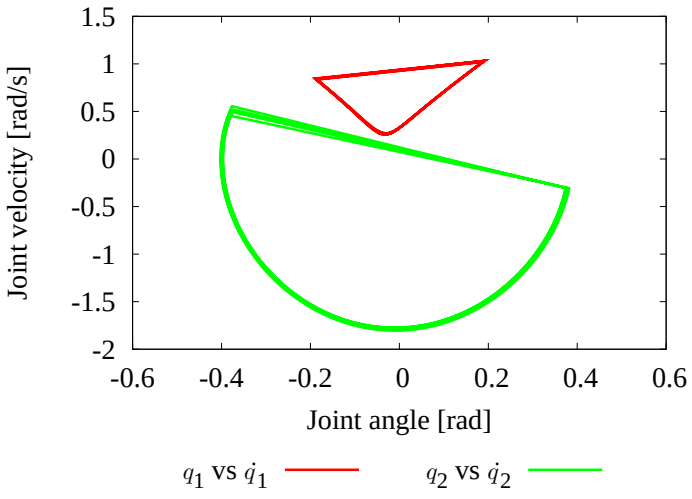

(c)

Fig. 2.7: Simulation results of VPDW where $\phi = 0.017$ rad: (a) control torque, (b) mechanical energy, (c) phase portrait.

2.4 Energy Feedback Control

The robustness of VPDW is very low, because VPDW doesn't include any feedback components with respect to the reference trajectory. As a possible approach, robust control based on tracking the energy trajectory of the PDW was proposed by Asano *et al.* [14]. This control method can stabilize planar compass biped walking based on the PDW concept. It is known from the features of planar PDW that the increasing rate of the mechanical energy E w.r.t the horizontal CoM position r_{Cx} is constant:

$$\frac{\partial E}{\partial r_{Cx}} = m_{tot} g \tan\phi. \tag{2.8}$$

Eq. (2.8) indicates that gravity component of the walking direction exists irrespective of position or orientation. This equation always can be realized.

The time differential of Eq (2.8) is:

$$\dot{E} = m_{tot} g \dot{r}_{Cx} \tan\phi, \tag{2.9}$$

where $\dot{r}_{Cx}$ is the horizontal component of the CoM velocity vector. This equation shows that the acceleration of the robot in the walking direction is concentrated at the CoM. Then, the desired energy trajectory E_d can be chosen as:

$$E_d(r_{Cx}) = m_{tot} g r_{Cx} \tan\phi + E_0, \tag{2.10}$$

where E_0 is the desired mechanical energy when $r_{Cx} = 0$ for stable walking. Asano *et al.* proposed the following asymptotic stabilizing control:

$$\frac{d}{dt}(E - E_d(r_{Cx})) = -\zeta(E - E_d(r_{Cx})), \tag{2.11}$$

where ζ is a constant positive feedback gain. Based on Eqs. (2.8) and (2.10), the time derivative of the energy error is:

$$\frac{d}{dt}(E - E_d(r_{Cx})) = \dot{\boldsymbol{q}}^T \boldsymbol{\tau} - m_{tot} g \dot{r}_{Cx} \tan\phi, \tag{2.12}$$

Therefore, based on Eqs. (2.11) and (2.12), we can solve the following indeterminate equation:

$$\begin{aligned} -\zeta(E - E_d(r_{Cx})) &= \dot{\boldsymbol{q}}^T \boldsymbol{\tau} - m_{tot} g \dot{r}_{Cx} \tan\phi, \\ \dot{\boldsymbol{q}}^T \boldsymbol{\tau} &= m_{tot} g \dot{r}_{Cx} \tan\phi - \zeta(E - E_d(r_{Cx})). \end{aligned} \tag{2.13}$$

As a solution, we choose the constant torque ratio condition:

$$\tau_1 = \mu \tau_2, \tag{2.14}$$

where μ is a constant ratio which can be derived from a torque ratio of the VPDW. The control torque ratio of the VPDW is:

$$\frac{\tau_1}{\tau_2} = \frac{(ma + m_h l + ml)\cos q_1 + mb\cos(q_1 + \pi + q_2)}{mb\cos(q_1 + q_2)}. \tag{2.15}$$

μ is the linearized approximation value of the torque ratio at the equilibrium point ($q_1 = q_2 = 0$):

$$\mu = \frac{(ma + m_h l + ml) - mb}{mb}, \tag{2.16}$$

$$= \frac{(ma + m_h l + ml)}{mb} - 1. \tag{2.17}$$

$$\tag{2.18}$$

The solution of Eq. (2.13) with constant torque ratio is:

$$\boldsymbol{\tau}_{ef} = \begin{bmatrix} \mu \\ 1 \end{bmatrix} \frac{m_{tot} g \dot{r}_{Cx} \tan\phi - \zeta(E - E_d(r_{Cx}))}{\mu \dot{q}_1 + \dot{q}_2}. \tag{2.19}$$

This control input is time-independent and maintains the property of autonomy which is the base for PDW. Figures 2.8 and 2.9 show the simulation results, where $\phi = 0.017$ rad, $\mu = -6.0$, $\zeta = 10.0$ s^{-1} and $E_0 = 149.7$ J. The biped model starts walking with unsuitable initial state. The initial state X_{ini} is in the neighborhood of the stable equilibrium point. It is possible to see that the mechanical energy is stabilized asymptotically to the desired energy trajectory by energy feedback control.

In order to examine the effectiveness of the energy feedback control in detail, we compared the results of $\zeta = 0\ \mathrm{s}^{-1}$ with results of $\zeta = 10\ \mathrm{s}^{-1}$. From Fig. 2.10, we can see that in case of $\zeta = 10\ \mathrm{s}^{-1}$, the step period converges to steady walking faster than that in case of $\zeta = 0\ \mathrm{s}^{-1}$ by energy feedback control.

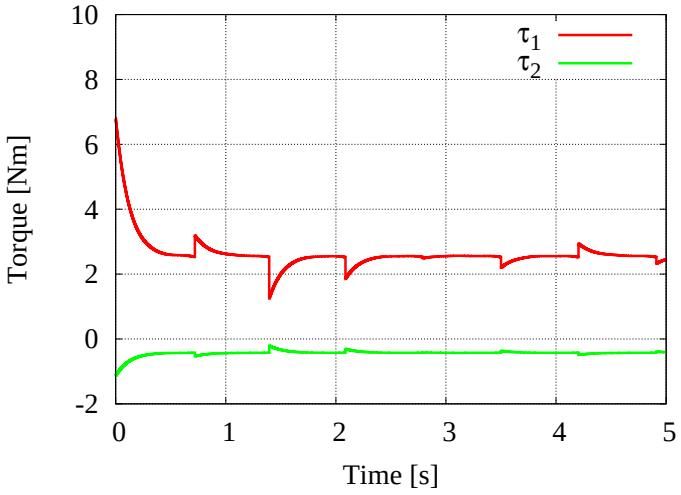

(a)

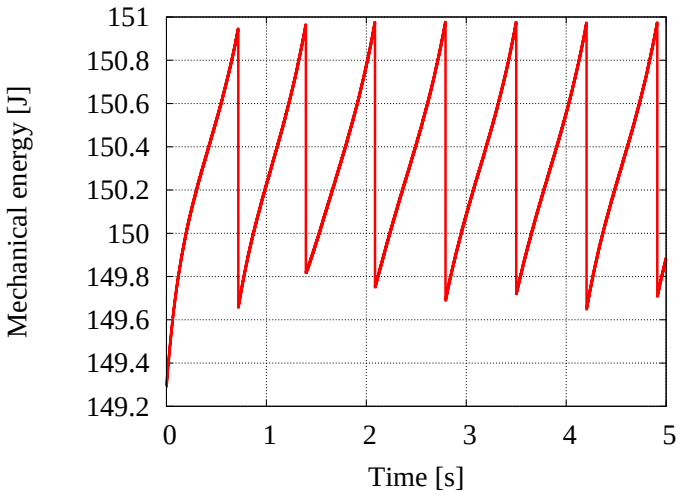

(b)

Fig. 2.8: Simulation results of Limit Cycle Walking by energy feedback control (1): (a) control torque, (b) mechanical energy.

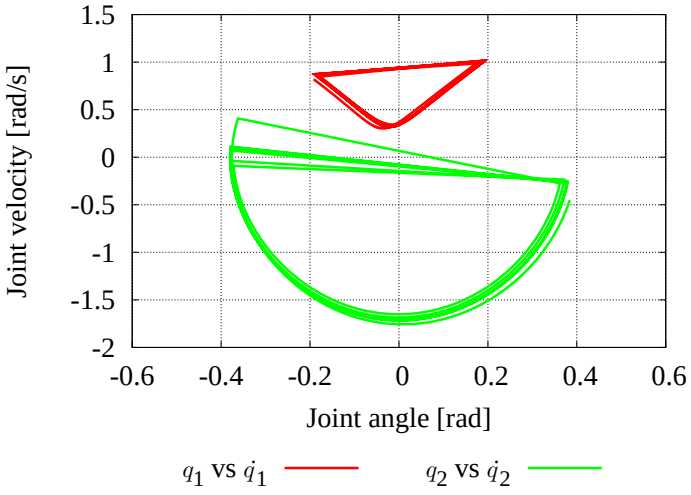

(a)

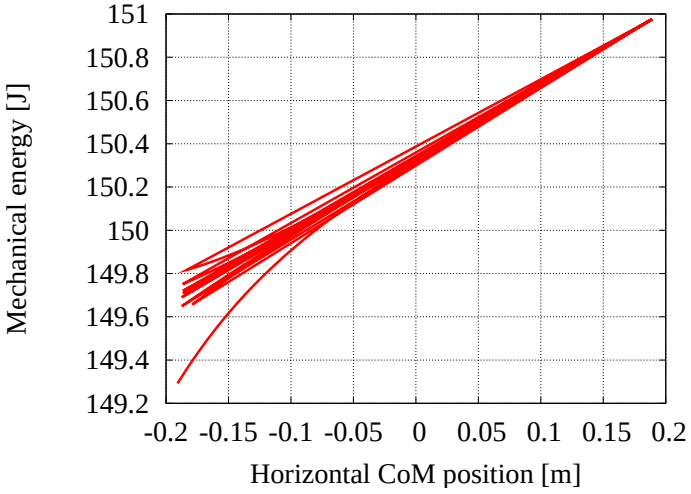

(b)

Fig. 2.9: Simulation results of Limit Cycle Walking by energy feedback control (2): (a) phase portrait, (b) relation between r_{Cx} and E.

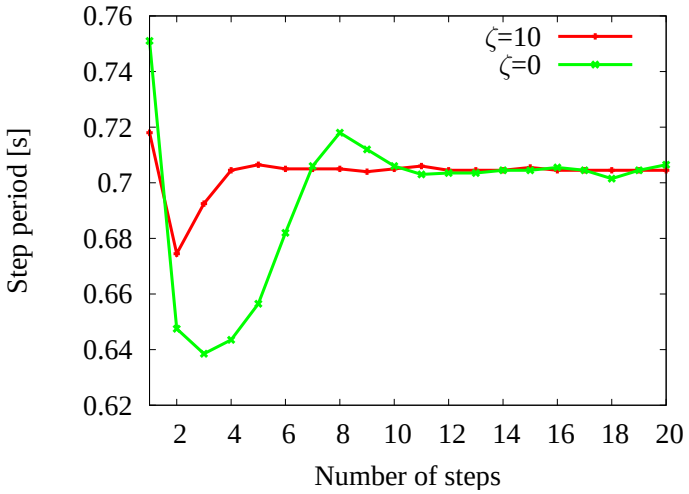

Fig. 2.10: Convergence of the step period.

2.5 Discussion and Conclusion

In this chapter, we introduced the basic mechanism of PDW from a view point of the mechanical energy.

PDW is generated by the interaction between the dynamics of the robot and the environment. On a shallow slope, the biped model can walk with a driving force $m_{tot}g\sin\phi$ in the walking direction obtained from the gravity field only. In other words, a driving force due to the gravity field always exists in the walking direction of the robot. Stable PDW is a periodic phenomenon. During the single support phase, the virtual mechanical energy is restored monotonically by the gravity field, on the other hand, at the instant of collision, the virtual mechanical energy dissipates discontinuously.

VPDW is a method which is imitating the mechanism of PDW. On even ground or gentle uphill, the robot can walk with a driving force $m_{tot}g\tan\phi$ obtained from the virtual gravity force as a control input. Therefore the

walking energy can be increased during the single support phase. This feature is the same as that of PDW.

The most important point of VPDW is that the increasing rate of the mechanical energy w.r.t. the position of the CoM $\frac{\partial E}{\partial r_{Cx}}$ coincides with the driving force $m_{tot}g\tan\phi$ in the walking direction (Eq. (2.8)). This feature always comes into existence irrespective of the number of links. Energy feedback control is a useful robust control method based on the PDW concept. At present, we think that this is the best feedback control method based on PDW. Consequently, it is possible to generate robust walking motion based on PDW (see Fig. 2.9). This control method is definitely a feedback control method, therefore the robot can absorb disturbances and changes in the environment. Possibilities for three-dimensional walking are discussed below, where this control method is applied as a sagittal motion stabilizer.

In this chapter, we dealt with a compass biped model which is the simplest possible model for understanding of basic mechanism of PDW. PDW has a simple mechanism (see Fig. 2.4). Eq. (2.8) represents the mechanism of acceleration in the walking direction. However, this equation is true only if the robot model is a compass biped. The walking pattern includes nonlinear phenomena and an uncertain mechanism of generation of the limit cycle. Therefore, it is difficult to put it into practical use. At present, nobody knows why a compass biped model can walk on a shallow slope. Nevertheless, we think that it is important to take full advantage of the fact from the viewpoint of engineering.

Chapter 3

Powered 2D Biped

Humanoid robots have many degrees of freedom (DOF). However, the compass biped model which we dealt with in Chapter 2 has only two DOF. Therefore, to apply the PDW based control to humanoid robots, we have to extend the biped model. In this chapter, we deal with various extended 2D biped models.

3.1 Biped Model with Ankle and Knee Joint

3.1.1 Biped model

Figure 3.1 shows the biped model which is dealt with in this section. The biped model is composed of six links. The physical parameters of the biped model are shown in Table 3.1. We assume the support leg to be always fixed to be ground. The generalized coordinates of the model are the joint angles: $\boldsymbol{q} = \begin{bmatrix} q_1 & q_2 & q_3 & q_4 & q_5 \end{bmatrix}^T$, while the generalized force vector is represented in terms of joint torque as $\boldsymbol{\tau} = \begin{bmatrix} \tau_1 & \tau_2 & \tau_3 & \tau_4 & \tau_5 \end{bmatrix}^T$.

3.1.2 Control based on a virtual biped model

Energy feedback control tracks a reference trajectory of the mechanical energy which depends on the CoM position (Eq. 2.8). In turn, the joint control

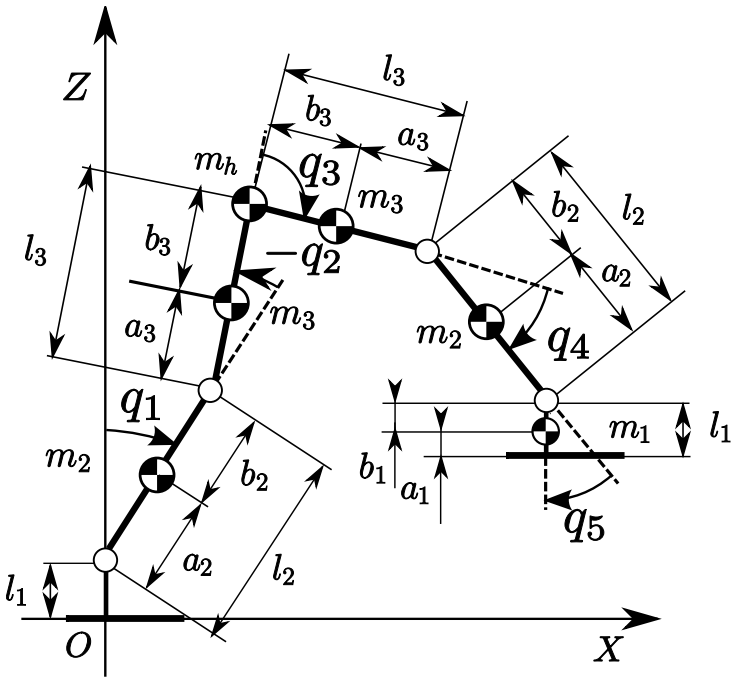

Fig. 3.1: Biped model with ankle and knee.

Table 3.1: Physical parameters of the biped model with ankle and knee.

Symbol	Parameter name	Value	
m_1	foot mass	0.309	kg
m_2	shank mass	0.286	kg
m_3	thigh mass	0.439	kg
m_h	hip mass	4.960	kg
l_1	foot length	0.037	m
l_2	shank length	0.10	m
l_3	thigh length	0.10	m
a_1	lower part of foot	0.028	m
b_1	upper part of foot	0.009	m
a_2	lower part of shank	0.057	m
b_2	upper part of shank	0.043	m
a_3	lower part of thigh	0.028	m
b_4	upper part of thigh	0.072	m

torques are calculated with the velocity of CoM (Eq. 2.9). Therefore, energy feedback control can generate a stable Limit Cycle Walking based on the PDW concept (see Figs. 2.8 and 2.9).

The feature of mechanical energy restoration, monotonically during the single support phase is always realized irrespective of the number of links of the biped model. Hence, we think that it is important to focus on the mechanical energy for extending the control method based on the PDW concept. However, energy feedback control is limited to a compass biped model.

As a possible approach, we try to extend energy feedback control with conventional control methods. In this section, we introduce the control method for the biped model with ankle and knee, based on a simple biped model. The simple biped model is called "virtual biped model". Figure 3.2 shows a block chart of the control method based on the virtual biped model dealt with in this section.

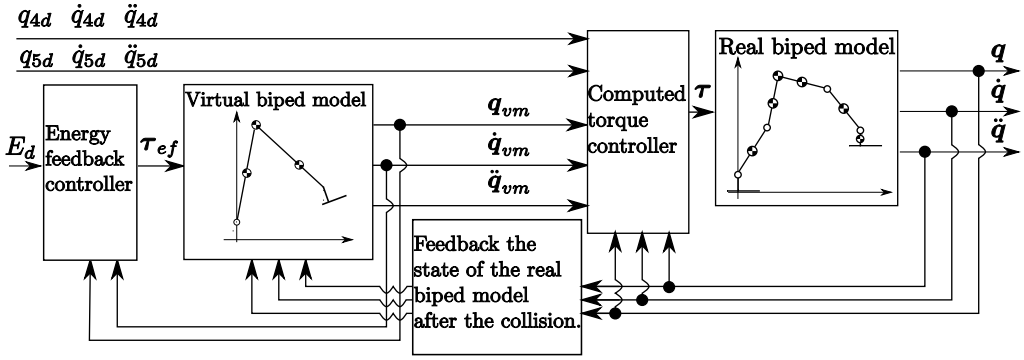

Fig. 3.2: Block chart of a controller based on energy feedback control with the virtual biped model.

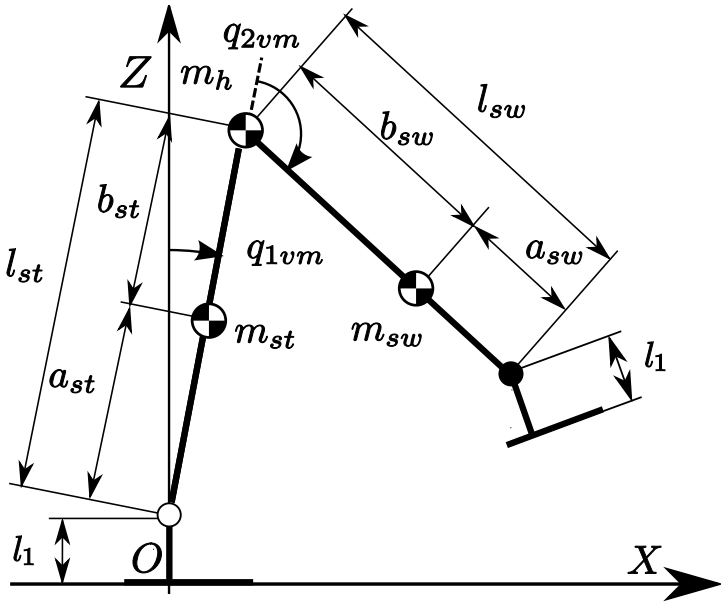

Fig. 3.3: Virtual biped model.

Virtual biped model for walking pattern generation

The biped model with ankle and knee has five DOF. On the other hand, the virtual biped model has only two DOF as shown in Fig. 3.3. The generalized coordinate vector is defined as $\boldsymbol{q}_{vm} = \begin{bmatrix} q_{1vm} & q_{2vm} \end{bmatrix}^T$.

The virtual biped model needs suitable mass properties for reducing the differences between the virtual biped model and the actual biped model. Especially, at the collision instant, the mass properties are very important because the discontinuous transformation of the joint velocities at the instant of collision are determined by a pre-collision angular momentum only. Therefore, this section sets the mass properties as follows:

$$m_{sw} = m_1 + m_2 + m_3, \tag{3.1}$$

$$l_{sw} = l_2 + l_3, \tag{3.2}$$

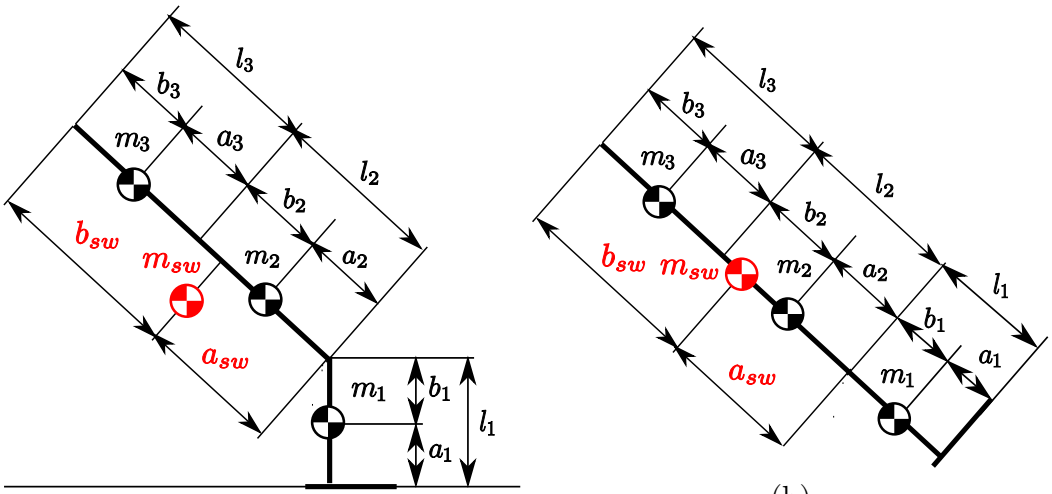

Fig. 3.4: Setting of swing leg CoM position of the virtual biped model: (a) ideal setting, (b) setting in this section.

$$a_{sw} = l_{sw} - b_{sw}, \tag{3.3}$$

$$b_{sw} = \frac{m_1(b_1 + l_2 + l_3) + m_2(b_2 + l_3) + m_3 b_3}{m_{sw}}. \tag{3.4}$$

In order to reduce the difference in the angular momenta of the virtual biped model and the actual biped model, the CoM position of the virtual biped model's swing leg should be defined based on pre-collision states of the actual biped model as shown in Fig. 3.4 (a), ideally. However, in the stage of setting the virtual biped model, it is impossible to know the pre-collision states of the actual biped model. Accordingly, we set the CoM position of the virtual biped model as shown in Fig. 3.4 (b) as the next best policy. However in case of setting as shown in Fig. 3.4 (b), the difference in the angular momenta of the virtual biped model and the actual biped model at the pre-collision state becomes larger with the length of the stride.

The DOF of the model equals that of a compass biped model which was dealt with in Chapter 2. Hence, the virtual biped model can track a reference

trajectory of the mechanical energy via energy feedback control similar to a compass biped model. The control torque vector of energy feedback control $\boldsymbol{\tau}_{ef}$ for the virtual biped model is:

$$\boldsymbol{\tau}_{ef} = \begin{bmatrix} \mu \\ 1 \end{bmatrix} \frac{m_{tot} g \dot{r}_{Cxvm} \tan\phi - \zeta(E - E_d(r_{Cxvm}))}{\mu \dot{q}_{1vm} + \dot{q}_{2vm}}, \tag{3.5}$$

where r_{Cxvm} denotes the horizontal CoM position of the virtual biped model. Consequently, the biped walking of the virtual biped model is stabilized based on the PDW concept. This section uses the control both for increasing robustness of the biped walking and achieving convergence of the errors due to the difference in the models. The reference trajectories of the ankle / knee joint of the stance leg and hip joint are determined based on the states of the virtual biped model.

Reference trajectory of the knee

The knee joint of the swing leg is controlled by tracking a reference trajectory. As a possible reference trajectory of the knee joint, this section chooses the following time variant-function, shown in Fig. 3.5. The reference trajectory of the knee joint q_{4d} is generated by a cubic sine function [9]:

$$q_{4d}(t) = \begin{cases} A \sin^3(\frac{\pi}{t_{f4}} t) & (t \leq t_{f4}) \\ 0 & (t > t_{f4}), \end{cases} \tag{3.6}$$

where A denotes the amplitude of knee motion, t_{f4} denotes the final time of knee joint and t is time. The trajectory has no energy dissipation because there is no collision in the knee joint.

Reference trajectory of ankle

The reference trajectory of the ankle joint of the swing leg is generated via the spline function:

$$q_{5d}(t) = \begin{cases} q_{5d}(t) = a_0 + a_1 t + a_2 t^2 + a_3 t^3 + a_4 t^4 + a_5 t^5 & (t \leq t_{f5}), \\ q_{5d-f} & (t > t_{f5}), \end{cases} \tag{3.7}$$

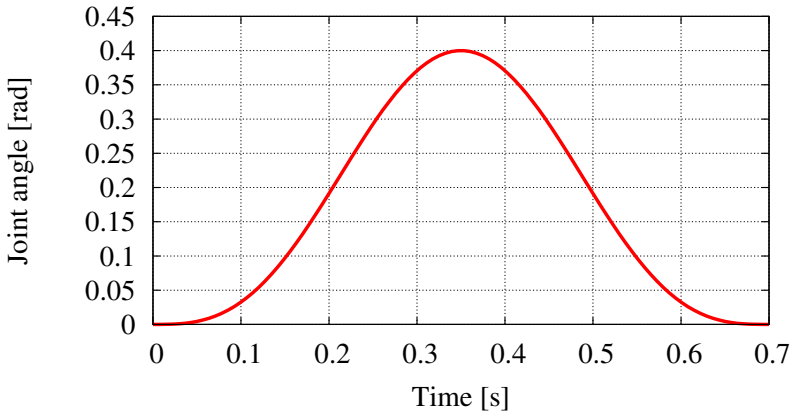

Fig. 3.5: Behavior of $A\sin^3\dfrac{\pi}{t_{f4}}t$.

where a_i, $i = 0, 1, ..., 5$ are the constant coefficients of the spline function, q_{5d-f} is a desired angle at the collision instant and t_{f5} denotes the final time. Note that, q_{5d-f} is calculated from the initial state because the stable PDW is periodic.

Tracking control

For strictly tracking, the states of the biped model from the reference trajectory, the control torques are calculated via a computed torque method:

$$\begin{aligned} \boldsymbol{\tau} &= \boldsymbol{M}(\boldsymbol{q})\boldsymbol{u} + \boldsymbol{C}(\boldsymbol{q}, \dot{\boldsymbol{q}})\dot{\boldsymbol{q}} + \boldsymbol{g}(\boldsymbol{q}), \\ \boldsymbol{u} &= \ddot{\boldsymbol{q}}_d + \boldsymbol{K}_p(\boldsymbol{q}_d - \boldsymbol{q}) + \boldsymbol{K}_d(\dot{\boldsymbol{q}}_d - \dot{\boldsymbol{q}}), \end{aligned} \tag{3.8}$$

where $\boldsymbol{q}_d = \begin{bmatrix} q_{1d} & q_{2d} & q_{3d} & q_{4d} & q_{5d} \end{bmatrix}^T$ denotes the reference trajectory, $\boldsymbol{K}_p = \text{diag}\begin{bmatrix} k_{p1} & k_{p2} & k_{p3} & k_{p4} & k_{p5} \end{bmatrix}$ and $\boldsymbol{K}_d = \text{diag}\begin{bmatrix} k_{d1} & k_{d2} & k_{d3} & k_{d4} & k_{d5} \end{bmatrix}$ are a

proportional gain and a differential gain respectively.

3.1.3 Numerical simulation

Figure 3.6 shows the simulation results of the biped model with ankle and knee joint, when $\phi = 0.01$ rad, $\zeta = 10$, $\mu = -8.27$ $A = 0.5$, $t_{f4} = 0.4$ s, $t_{f5} = 0.4$ s, $\boldsymbol{K}_p = \mathrm{diag}\begin{bmatrix}500 & 500 & 500 & 500 & 500\end{bmatrix}$ s^{-2} and $\boldsymbol{K}_d = \mathrm{diag}\begin{bmatrix}50 & 50 & 50 & 50 & 50\end{bmatrix}$ s^{-1}. Figure 3.6 (a) shows the control torque. From this figure, it is seen that the control torques aren't flat. The control torque for the hip joint is the largest of them. We think that the hip joint needs large torque due to the coexistence of knee joint control and energy feedback control. Figure 3.6 (b) shows the mechanical energy. From the shape of the graph, we see that the mechanical energy doesn't increase monotonically during the single support phase such as in PDW. Therefore, this control method doesn't satisfy the feature about mechanical energy restoration of PDW. From Fig. 3.6 (c), we can see that the walking pattern is periodic, which is similar to PDW (see Fig. 2.5 (c)).

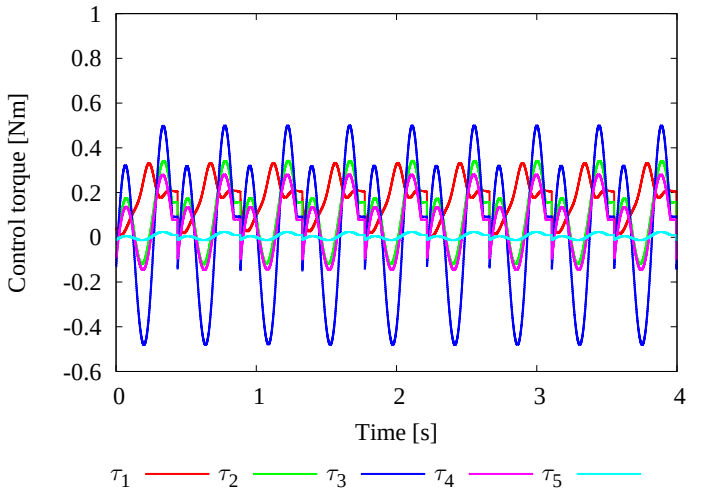

(a)

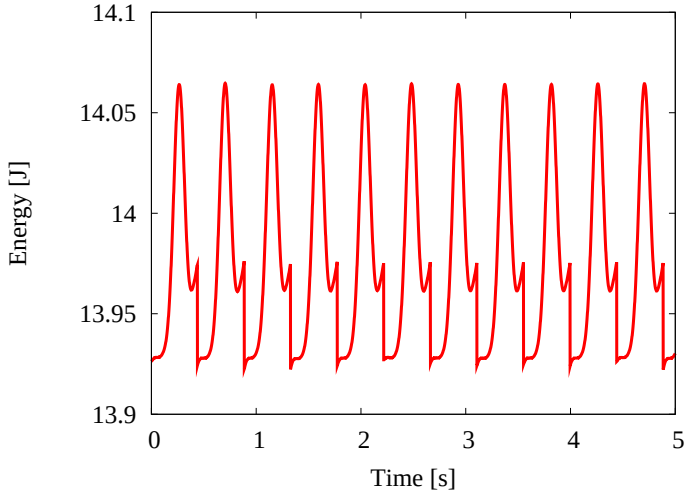

(b)

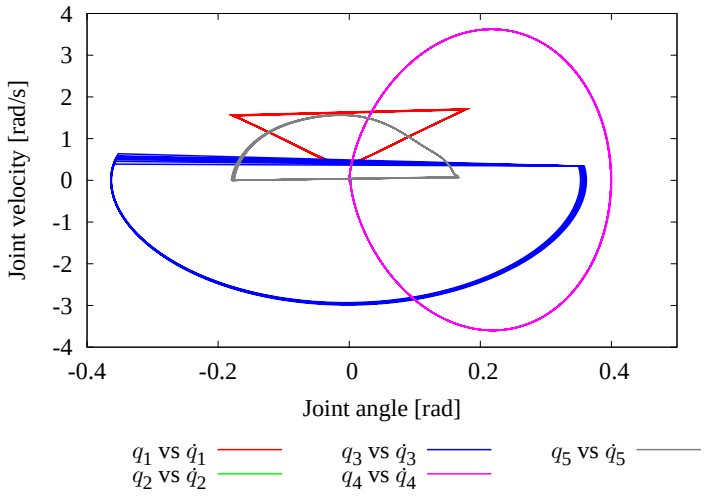

(c)

Fig. 3.6: Simulation results of energy feedback control with the virtual biped model: (a) control torque, (b) mechanical energy, (c) phase portrait.

3.2 Biped Model with Upper Body

Passive-dynamic walkers generally have only lower limbs without upper body. However humanoid robots need an upper body because they are required to assist us by using their upper limbs. Therefore we have to consider how to add an upper body to a passive dynamic biped model.

This section deals with the 2D biped model with ankle, knee joint of the swing leg and upper body in sagittal plane as shown in Fig. 3.7. The physical parameters of the biped model are shown in Table 3.2. The model is composed of five joints and six links. We assume that the stance leg is always fixed to the ground. We also assume that link inertia moments and joint friction can be ignored. The generalized coordinates of the model are the joint angles: $\boldsymbol{q} = \begin{bmatrix} q_1 & q_2 & q_3 & q_4 & q_5 \end{bmatrix}^T$, while the generalized force vector is represented in terms of joint torque as $\boldsymbol{\tau} = \begin{bmatrix} \tau_1 & \tau_2 & \tau_3 & \tau_4 & \tau_5 \end{bmatrix}^T$.

3.2.1 Virtual Passive Dynamic Walking

This subsection introduces the control method for the biped model described above based on the PDW concept.

The ankle joint of the stance leg, the hip joint and the knee joint are controlled by VPDW. The mechanical energy restoration of VPDW is:

$$\dot{\boldsymbol{q}}^T \boldsymbol{\tau}_{vg} = m_{tot} g \dot{r}_{Cx} \tan\phi, \tag{3.9}$$

where $\boldsymbol{\tau}_{vg} = \begin{bmatrix} \tau_{vg1} & \tau_{vg2} & \tau_{vg3} & 0 & 0 \end{bmatrix}$ denotes the control torque for VPDW. In the case of the 2D biped model with knee joint, the joint torque values are resolved by the following indeterminate equation:

$$\dot{q}_1 \tau_{vg1} + \dot{q}_2 \tau_{vg2} + \dot{q}_3 \tau_{vg3} = m_{tot} g \dot{r}_{Cx} \tan\phi. \tag{3.10}$$

To solve Eq. (3.10), we adopt an independent control for the knee joint firstly. This approach seeks a beneficial use of redundancy, which also solves the *foot-scuffing* problem. Consequently, the knee joint is controlled by PID control,

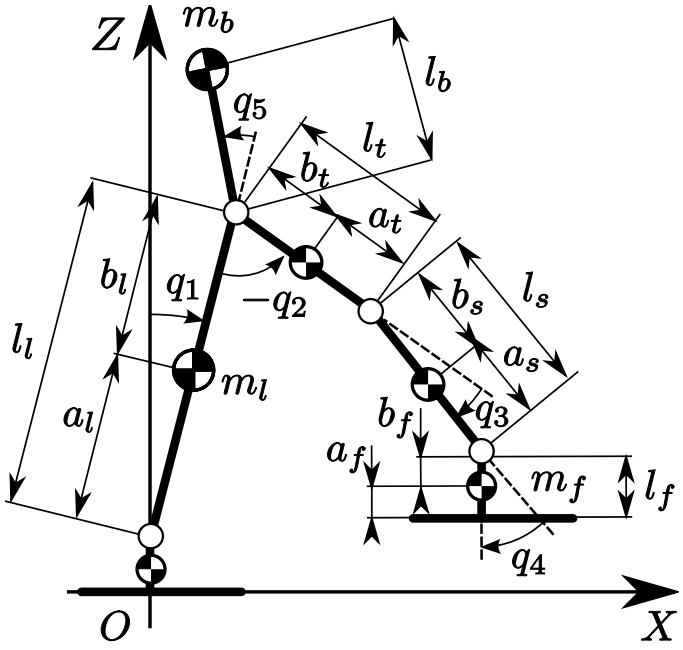

Fig. 3.7: Biped model with ankle, knee joint and upper body.

which tracks a reference trajectory:

$$\tau_{vg3} = k_d(\dot{q}_{3d} - \dot{q}_3) + k_p(q_{3d} - q_3) + k_i \int (q_{3d} - q_3)dt, \tag{3.11}$$

where q_{3d} is the reference trajectory for the joint angle of the knee. As a reference trajectory for the knee joint, we may chose the following:

$$q_{3d}(t) = \begin{cases} A\sin^3(\frac{\pi}{T}t) & (t \leq T) \\ 0 & (t > T) \end{cases}, \tag{3.12}$$

where A is the amplitude and T is the steady step period. This function permits smooth motion of the knee joint and avoids energy loss during kneestrike.

Secondly, we consider an independent control for the ankle joint. As a possible approach, we apply ZMP control, because the robot can be stabilized. In case of point contact between the stance leg's toe and the ground,

Table 3.2: Physical parameters of the biped model with ankle, knee and upper body.

Symbol	Parameter name	Value	
m_l	leg mass	5.0	kg
m_s	shank mass	2.5	kg
m_t	thigh mass	2.5	kg
m_f	foot mass	10.0	kg
m_b	upper body mass	5.0	kg
l_l	leg length	1.0	m
l_s	shank length	0.5	m
l_t	thigh length	0.5	m
l_f	foot length	0.2	m
l_b	upper body length	0.5	m
a_l	lower part of leg	0.5	m
b_l	upper part of leg	0.5	m
a_s	lower part of shank	0.25	m
b_s	upper part of shank	0.25	m
a_t	lower part of thigh	0.25	m
b_t	upper part of thigh	0.25	m
a_f	lower part of foot	0.1	m
b_f	upper part of foot	0.1	m

the ZMP can be calculated from:

$$\text{ZMP} = -\frac{\tau_{vg1}}{R_n}, \tag{3.13}$$

where R_n is the ground reaction force. Using the reference ZMP position x_d, the joint torque τ_{vg1} of the ankle joint becomes:

$$\tau_1 = -R_n x_d. \tag{3.14}$$

By substituting Eqs. (3.11) and (3.13) into Eq. (3.10), the hip joint torque τ_{vg2} becomes:

$$\tau_{vg2} = \frac{m_{tot} g \dot{r}_{Cx} \tan\phi - \dot{q}_1 \tau_1 - \dot{q}_3 \tau_3}{\dot{q}_2}. \tag{3.15}$$

However, τ_{vg2} has a singular point at $\dot{q}_2 = 0$. Therefore, it is necessary to change the control method to avoid the singularity. To deal with the singularity, we adopt a solution which determines the hip joint torque as $\tau_{2vg} = \tau_{2vgd}$, initially. Consequently, the ankle joint torque τ_{vg1} becomes:

$$\tau_{vg1} = \frac{m_{tot} g \dot{r}_{Cx} \tan\phi - \dot{q}_2 \tau_{vg2} - \dot{q}_3 \tau_{vg3}}{\dot{q}_1}. \tag{3.16}$$

In the case of PDW based control, $\dot{q}_1$ is generally positive. On the other hand, the hip joint torque τ_{vg2d} is calculated as:

$$\tau_{vg2d} = \eta \dot{q}_2, \tag{3.17}$$

where η is a constant positive feedback gain. Just before switching the control method, the desired hip joint torque is:

$$\tau^{-}_{vg2d} = \frac{m_{tot} g \dot{r}_{Cx} \tan\phi - \dot{q}_1 \tau_{vg1} - \dot{q}_3 \tau_{vg3}}{\dot{q}_2}. \tag{3.18}$$

After switching, it becomes:

$$\tau^{+}_{vg2d} = \eta \dot{q}_2. \tag{3.19}$$

To obtain smooth switching, η is derived as:

$$\eta = \frac{m_{tot} g \dot{r}_{Cx} \tan\phi - \dot{q}_1 \tau^{-}_{vg1} - \dot{q}_3 \tau^{-}_{vg3}}{\dot{q}_2^2}. \tag{3.20}$$

In this section, we control the upper body link and the foot of the swing leg based on the Lagrange multiplier method for stable walking. The upper body motion influences the stability of the walking. On the other hand, it is necessary that the foot of the swing leg is parallel to the floor at the collision instant. Therefore we set the following constraint $\boldsymbol{\tau}_c$ for the control of the upper body and the ankle joint of the swing leg:

$$\boldsymbol{\tau}_c = \boldsymbol{J}_M^T \boldsymbol{\lambda}_C, \tag{3.21}$$

$$\boldsymbol{J}_M \dot{\boldsymbol{q}} = \boldsymbol{0},$$

$$\boldsymbol{J}_M = \begin{bmatrix} 1 & 0 & 0 & 0 & 1 \\ 1 & 1 & 1 & 1 & 0 \end{bmatrix}. \tag{3.22}$$

With the constraint calculated through the above equation $\boldsymbol{\tau}_c$, thereby the upper body keeps vertical orientation w.r.t. the floor, not destroying the stable walking. The foot of the swing leg also conserves the parallel orientation to the floor consistently with the control torque, as we can't know exactly when the foot collides with the floor.

Figure 3.8 shows the simulation results of VPDW, where $\phi = 0.02$ rad, $T = 0.75$ s, $A = 0.4$ rad, $x_d = -0.015$ m, $k_p = 300$ Nm/rad, $k_d = 30$ Nms/rad, $k_p = 1000$ Nm/rads and the timing of the control method switching from Eq. (3.15) to Eq. (3.16) is at $r_{cx} = 0.1$ m. Figure 3.8 (a) shows that the control torques for VPDW of the biped model aren't flat. This feature isn't similar to PDW of the compass biped model (see Fig. 2.5 (a)). On the other hand, we can see that the mechanical energy increases monotonically during the single support phase as shown in Fig.3.8 (b). This feature is similar to that with the compass biped model's PDW (see Fig. 2.5 (b)). This is because the control dealt with in this section is constructed based on Eq. (3.9). From the phase portrait (Fig.3.8 (c)), we can see that the biped model can indeed walk stably and periodically. Consequently, we can conclude that it is possible to generate biped walking of the biped model with the upper body by using combination of VPDW and geometric constraint.

3.2.2 Energy feedback control

In order to achieve robustness, we apply the energy feedback control to the biped model with upper body. We control the simple planar biped model (virtual biped model) with energy feedback control. The parameters of the simple planar biped model are based on the biped model with upper body. The virtual biped model is shown in Fig 3.9. We propose walking pattern generation based on stable limit cycle of the virtual biped model. The generalized coordinates of the virtual model are the joint angles: $\hat{\boldsymbol{q}} = \begin{bmatrix} \hat{q}_1 & \hat{q}_2 & \hat{q}_5 \end{bmatrix}^T$, while the relation between the generalized coordinate frame of the biped model $\boldsymbol{q}$

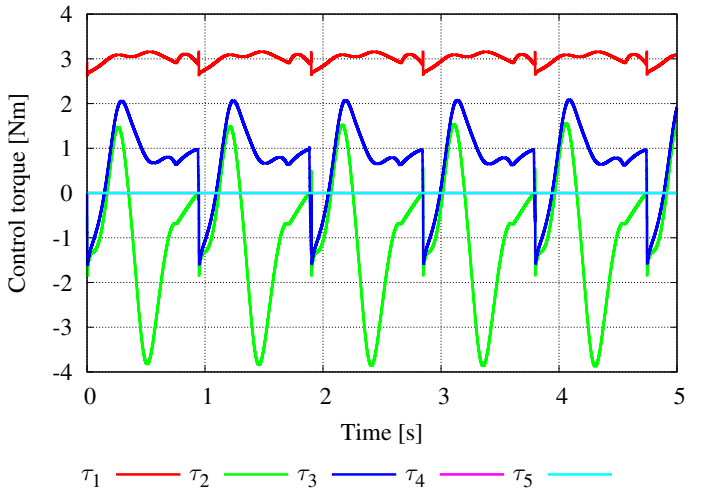

(a)

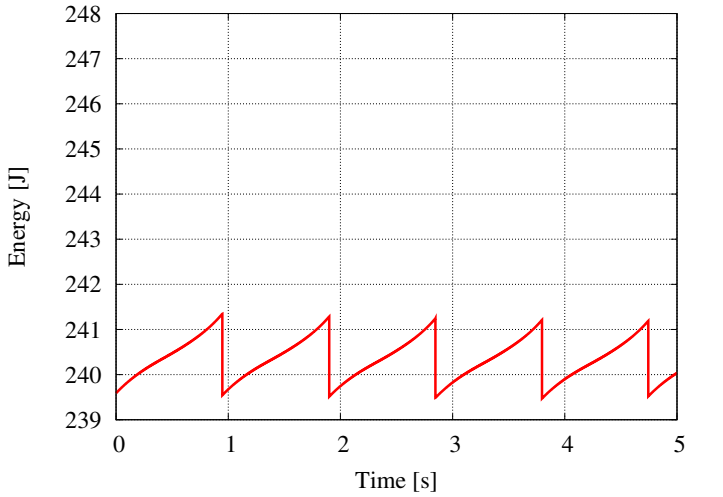

(b)

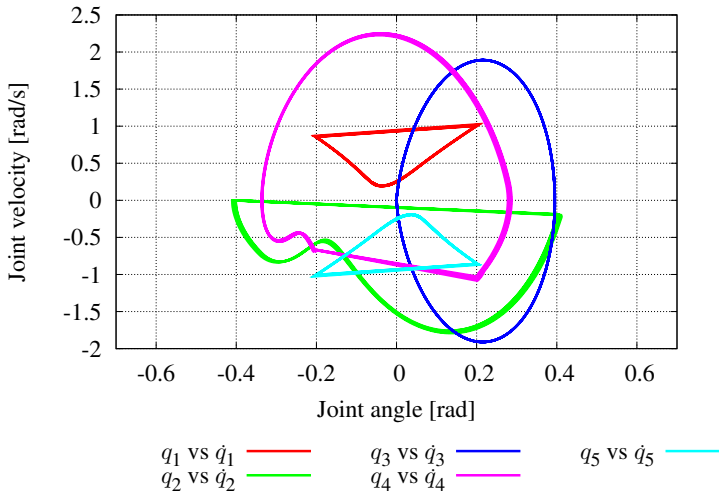

(c)

Fig. 3.8: Simulation results of the VPDW: (a) control torque for VPDW $\boldsymbol{\tau}_{vg}$ and knee joint control, (b) mechanical energy, (c) phase portrait.

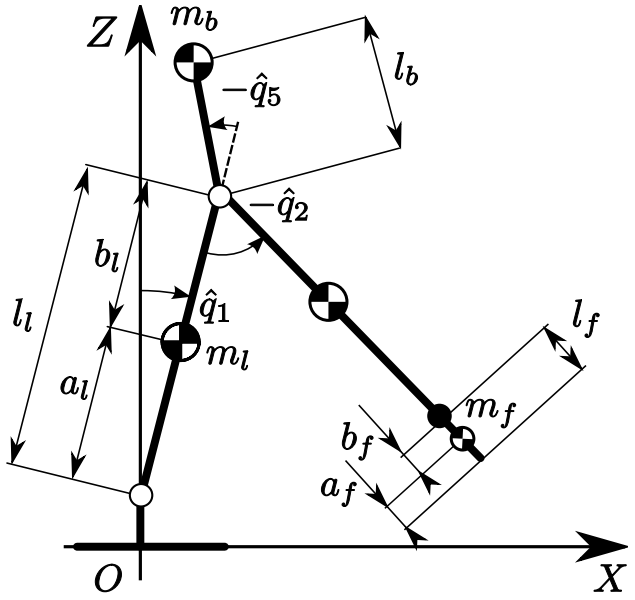

Fig. 3.9: Virtual biped model of the biped model with the upper body.

and $\hat{\boldsymbol{q}}$ is:

$$\begin{aligned} \hat{\boldsymbol{q}} &= \boldsymbol{S}\boldsymbol{q} \\ \boldsymbol{S} &= \begin{bmatrix} 1 & 0 & 0 & 0 & 0 \\ 0 & 1 & 0 & 0 & 0 \\ -1 & 0 & 0 & 0 & 0 \end{bmatrix}. \end{aligned} \tag{3.23}$$

The above equation means that the orientation of the upper body of the virtual biped model is always vertical w.r.t. the ground. Therefore, the virtual biped model has only 2DOF. The control torque of energy feedback control for the virtual biped model is calculated based on the relation between the horizontal CoM position and the mechanical energy (see Section 2.4).

Figure 3.10 shows the numerical simulation results of the biped model where $\phi = 0.02$ rad, $T = 0.8$ s, $A = 0.3$ rad, $k_p = 300$ Nm/rad, $k_d = 30$ Nms/rad, $k_p = 1000$ Nm/rads, $\zeta = 80t$ and $\mu = -5.5$, $E_0 = 240$ J. We can see that the control torque of energy feedback isn't similar to that of VPDW from

Fig. 3.10 (a). The control torque is relatively large. From Fig. 3.10 (b), it seems that the mechanical energy doesn't increase monotonically. The main cause of these features is the coupling between the tracking control of the knee joint and the energy feedback control. The above control tries to converge the mechanical energy of the virtual biped model with the reference trajectory. On the other hand, the knee joint state tracks the reference trajectory based on the time variant function. Figure 3.10 (c) shows the phase portrait. From this figure, we can confirm that the biped model can indeed walk periodically.

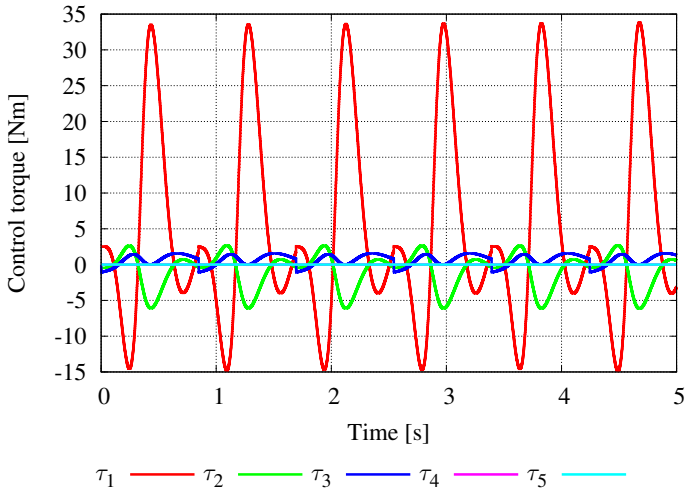

(a)

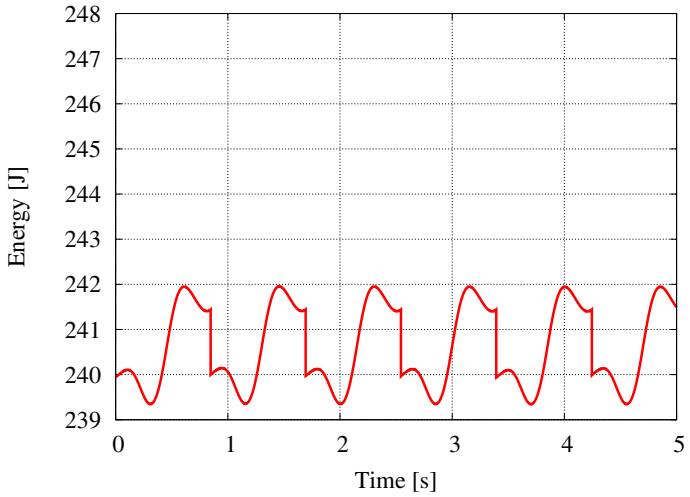

(b)

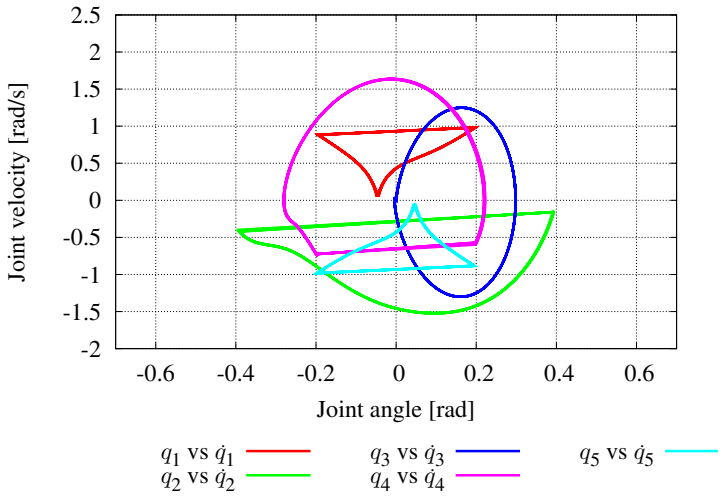

(c)

Fig. 3.10: Simulation results of the energy feedback control: (a) control torque for energy feedback control and knee joint control $\boldsymbol{\tau}_{ef}$, (b) mechanical energy, (c) phase portrait.

3.3 Discussion and Conclusions

In this chapter, we dealt with two extended 2D biped models (see Fig. 3.1, 3.7). We can generate their walking pattern based on the energy feedback control. These extended 2D biped models can be used as a sagittal walking pattern generators for walking pattern generation of 3D biped models, as will be described in Chapter 4.

The biped model with ankle and knee joint can walk under feedback control based on the virtual biped model. As shown in Fig. 3.6 (b), this control doesn't satisfy the feature of PDW because the walking pattern of the actual biped model is generated based on the virtual biped model's limit cycle. We have to optimize the reference trajectory of the knee joint from the view point of energy efficiency.

Stable VPDW of a biped model with ankle, knee and upper body can be realized. Passive-dynamic walkers generally have only lower limbs without upper body. Some researchers reported that energy efficiency of dynamic walking got worse as a result of adding an upper body [15] [16]. However, it is necessary to add an upper body to the biped model because the aim of our study is to apply the limit cycle based control to humanoid robots. They are required to help us by using their upper limbs. In this chapter, we used constraint torque to keep the upper body upright under the influence of gravity. Therefore it was easy to generate stable walking. However humanoid robots don't have special constraint mechanism generally. Therefore, in the stage when we have to apply the control to actual humanoid robots, we have to consider how to keep the upper body orientation without geometric constraint by using joint torque.

The energy feedback control based on the virtual biped model for the biped model with ankle, knee and upper body can generate stable walking pattern. However, compared to VPDW, this control needs large control

torque because there is coupling from each control. As a merit of this control, we can conclude that it is easy to find a stable limit cycle. The stability of limit cycle based walking depends on the system parameters and initial conditions. We expect that the control method with virtual biped model, will enable us to generate stable walking patterns for complex biped models. Hence, the next chapter uses this method for sagittal walking generation of 3D biped models.

Chapter 4

Powered 3D Biped

This is the main chapter of this thesis. The final aim of our study is to apply the Limit Cycle Walking based control to actual humanoid robots (see Chapter 1). Humanoid robots have many DOF and operate in 3D space. However, studies of 3D Limit Cycle Walking are rare, especially there are no studies focusing on the application to humanoid robots. We think that the desired features for biped walking, such as energy efficiency and naturalness, can be ensured via the Limit Cycle Walking concept, because this concept is to use the dynamics of the robots and the environment. Therefore, in the past, we proposed a walking pattern generator for the simplest 3D biped model as a combination of decoupling control, energy feedback control and so on [13]. This chapter firstly, explains the fundamentals of 3D PDW. Secondly, we propose a 3D walking pattern generator for two extended biped models based on energy feedback control from a virtual biped model. Via numerical simulations, we show that we can generate a stable walking pattern by extending our previous control method.

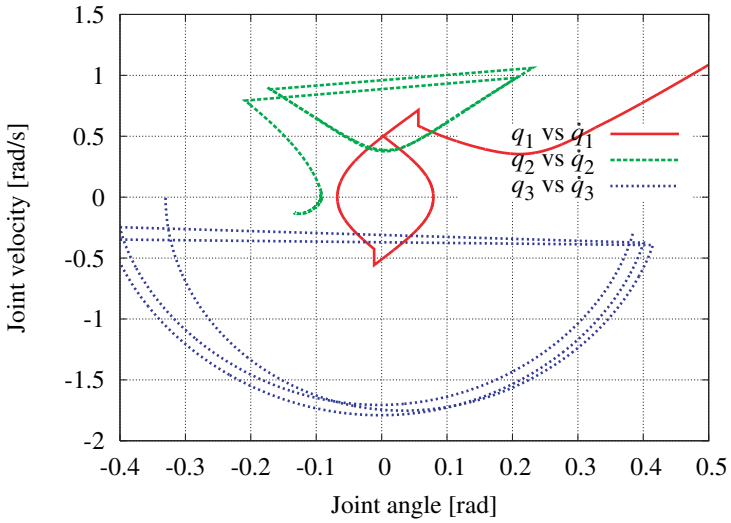

Fig. 4.1: Phase portrait of 3D Passive Dynamic Walking.

4.1 Fundamentals of Three-Dimensional Passive Biped Walking

Figure 4.1 shows the phase portrait of 3D PDW of the simplest biped model, as shown in Fig. 4.2 where the slope angle $\phi = 0.02$ rad. As shown this figure, PDW in 3D is impossible because the roll motion in the frontal plane cannot be energized by the gravity field. Consequently, there is no stable limit cycle. Therefore, we have to design a special control law for the roll motion. In addition, 3D biped walking based on the PDW concept has also the following inherent problems:

- it is very difficult to find a stable limit cycle of the 3D biped model because no explicit relation between initial conditions and stability are known;

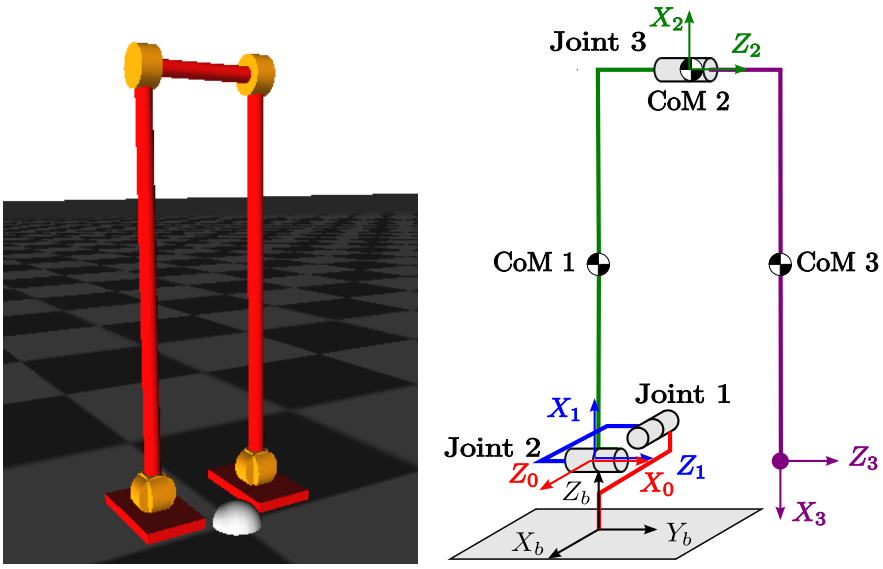

(a) (b)

Fig. 4.2: The simplest 3D biped model: (a) rendered view, (b) kinematic structure with coordinate frames.

- roll motion is coupled with pitch motion in the sagittal plane, therefore the limit cycle for pitch motion disappears;
- roll motion must be synchronized with pitch motion within the existing limit cycle.

Especially, coupling is an important issue. Therefore, it is necessary to compensate the roll and yaw motion [5], [12].

4.2 Biped Model with Knee

4.2.1 Biped model

This Section deals with a 3D biped model with knee joint as shown in Fig. 4.3. The physical parameters of the biped model are shown in Table 4.1. The model is composed of four joints and four links, including a stance leg, a thigh and a shank of the swing leg, and a pelvis. The four joints are the roll and pitch ankle joints of the stance leg, the hip pitch joint with 1DOF, and the knee joint of the swing leg with 1DOF. We also assume the following conditions:

- walking consists of two phases of motion: single support and double support;
- the stance leg is always fixed to the ground;
- leg switching occurs instantaneously during the double support phase;
- link inertia moment and joint friction can be ignored;
- there are foot links whose thickness and mass can be ignored.

The generalized coordinates of the model are the joint angles: $\boldsymbol{q} = \begin{bmatrix} q_1 & q_2 & q_3 & q_4 \end{bmatrix}^T$, while the generalized force vector is represented in terms of joint torque as $\boldsymbol{\tau} = \begin{bmatrix} \tau_1 & \tau_2 & \tau_3 & \tau_4 \end{bmatrix}^T$.

4.2.2 Walking generation and control

In the past, we proposed a method for stable walking pattern generation via a simple planar robot model [13]. In this section, we extend the controller to generate a stable walking pattern generator for the 3D biped model with knee joint. The block diagram of the control method is shown in Fig. 4.4. The control torque for the generation of the stable walking pattern is:

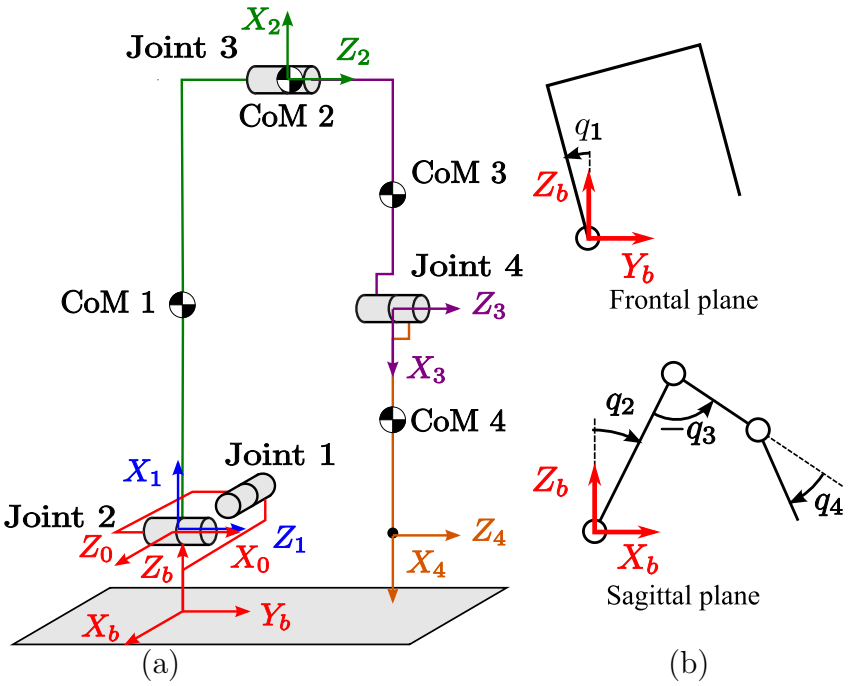

Fig. 4.3: 3D biped model with knee joint: (a) kinematic structure with coordinate frames, (b) generalized coordinates of the model.

$$\boldsymbol{\tau} = \boldsymbol{\tau}_{dcp} + \boldsymbol{\tau}_g + \boldsymbol{\tau}_{ef} + \boldsymbol{\tau}_{lock} + \boldsymbol{\tau}_{knee} + \boldsymbol{\tau}_{roll}, \tag{4.1}$$

where $\boldsymbol{\tau}_{dcp}$ denotes the joint torque for decoupling control torque which can be computed from $\boldsymbol{M}(\boldsymbol{q})$ and $\boldsymbol{C}(\boldsymbol{q}, \dot{\boldsymbol{q}})$, which are included in the motion equation, $\boldsymbol{\tau}_g$ denotes the joint torque for reconstruction of the gravity environment, $\boldsymbol{\tau}_{ef}$ denotes the torque for energy feedback control, $\boldsymbol{\tau}_{lock}$ denotes the hip locking torque for synchronization between the motions in the frontal and sagittal planes, $\boldsymbol{\tau}_{knee}$ denotes the control torque for the PD control of the knee joint, $\boldsymbol{\tau}_{roll}$ denotes the control torque for stabilization of the motion in the frontal plane. In the past, we proposed two reference trajectory generation methods for the motion in the frontal plane (spline function method and empirical method) [13]. In this chapter, we use the empirical method

Table 4.1: Physical parameters of the 3D biped model with knee joint.

Link name	Length [m]	Mass [kg]
Stance leg	$l_l = 1.0$	$m_l = 5.0$
Thigh	$l_t = 0.5$	$m_t = 2.5$
Shank	$l_s = 0.5$	$m_s = 2.5$
Pelvis	$l_p = 0.3$	$m_p = 10.0$

based on analysis of the collision equation.

We describe the details of these controls in subsequent sections.

Energy feedback control and 2D compass biped model

We describe walking pattern generation based on the stable limit cycle of the 2D simple biped model (virtual biped model) because it is difficult to find stable limit cycle of a 3D complex biped model empirically. This control method stabilizes planar compass biped walking based on the Passive Dynamic Walking concept (see Section 2.4). We control the virtual biped model with energy feedback control. The parameters of the virtual biped biped model are based on the 3D biped model. The virtual biped model is shown in Fig 4.5. We propose walking pattern generation based on the stable limit cycle of the 2D compass biped model. The generalized coordinates of the 2D compass biped model are the joint angles: $\hat{\boldsymbol{q}} = \begin{bmatrix}\hat{q}_2 & \hat{q}_3\end{bmatrix}^T$, while the relation between $\boldsymbol{q}$ and $\hat{\boldsymbol{q}}$ is:

$$\begin{aligned} \hat{\boldsymbol{q}} &= \boldsymbol{S}\boldsymbol{q} \\ \boldsymbol{S} &= \begin{bmatrix} 0 & 1 & 0 & 0 \\ 0 & 0 & 1 & 0 \end{bmatrix}. \end{aligned} \tag{4.2}$$

The joint torque for energy feedback control can be calculated as

$$\boldsymbol{u}_{ef} = \begin{bmatrix}\mu \\ 1\end{bmatrix} \frac{m_{tot} g \dot{r}_{Cx} \tan\phi - \zeta(E - E_d(r_{Cx}))}{\mu\dot{q}_2 + \dot{q}_3}, \tag{4.3}$$

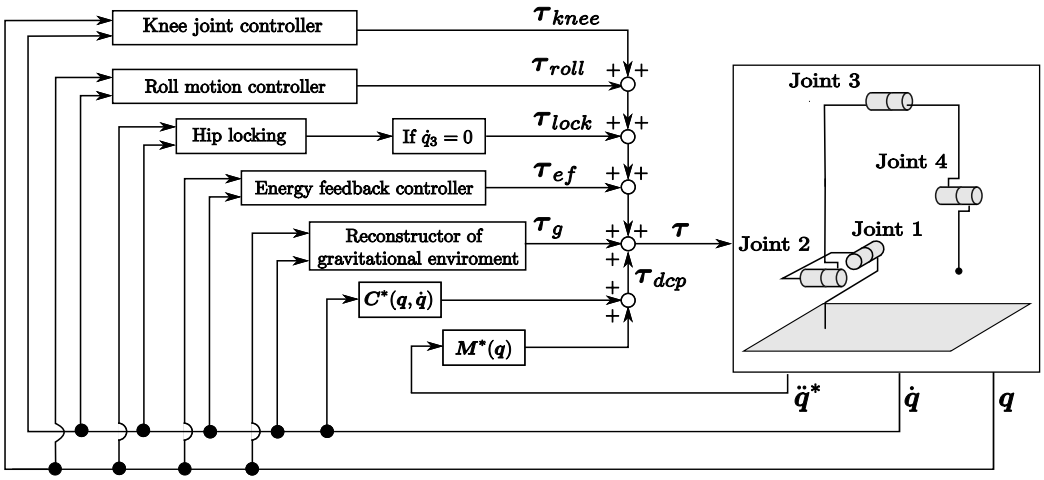

Fig. 4.4: Block diagram of biped controller based on the decoupling control and the energy feedback control.

where m_{tot} denotes the robot total mass, g denotes the gravity acceleration, ϕ denotes the virtual slope angle, E denotes the mechanical energy of the 2D compass biped model, E_d denotes the desired energy trajectory, r_{Cx} is the horizontal CoM position, ζ is the gain, and μ is the control torque ratio. The energy feedback control torque for the 3D biped model with knee joint becomes:

$$\boldsymbol{\tau}_{ef} = \begin{bmatrix} 0 \\ \boldsymbol{u}_{ef} \\ 0 \end{bmatrix}. \tag{4.4}$$

Decoupling control

The coupling between 2D motion in the sagittal plane and roll and yaw motion is very important issue for stable 3D walking generation as described above. Therefore, we have proposed a decoupling control law, which cancels the coupling between roll motion in the frontal plane and pitch motion in the sagittal plane. The biped model, which is controlled by this decou-

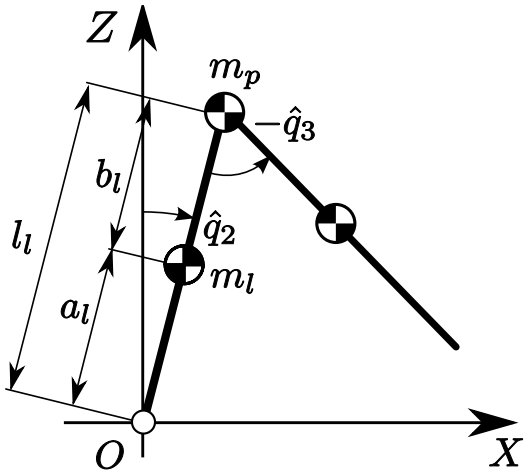

Fig. 4.5: 2D compass biped model.

pling control, doesn't need any special mechanisms for the compensation (e.g. semicircular feet) because this control is realized with joint actuation.

The decoupling control torque is calculated from the matrices $\boldsymbol{M}(\boldsymbol{q})$ and $\boldsymbol{C}(\boldsymbol{q}, \dot{\boldsymbol{q}})$ which are included in the motion equation:

$$\boldsymbol{M}(\boldsymbol{q}) = \begin{bmatrix} M_{11} & \cdots & M_{14} \\ \vdots & \ddots & \vdots \\ M_{41} & \cdots & M_{44} \end{bmatrix}, \tag{4.5}$$

$$\boldsymbol{C}(\boldsymbol{q}, \dot{\boldsymbol{q}}) = \begin{bmatrix} C_{11} & \cdots & C_{14} \\ \vdots & \ddots & \vdots \\ C_{41} & \cdots & C_{44} \end{bmatrix}. \tag{4.6}$$

The second to the fourth rows of the equation of motion describe the moments on the pitch joints (Joints 2, 3 and 4). The first column of these three rows describes the coupling moment due to the roll joint (Joint 1). Therefore, the

matrices for decoupling control become:

$$\boldsymbol{M}^*(\boldsymbol{q}) = \begin{bmatrix} 0 & M_{12} & M_{13} & M_{14} \\ M_{21} & 0 & 0 & 0 \\ M_{21} & 0 & 0 & 0 \\ M_{21} & 0 & 0 & 0 \end{bmatrix}, \tag{4.7}$$

$$\boldsymbol{C}^*(\boldsymbol{q}, \dot{\boldsymbol{q}}) = \begin{bmatrix} 0 & C_{12} & C_{13} & C_{14} \\ C_{21} & 0 & 0 & 0 \\ C_{21} & 0 & 0 & 0 \\ C_{21} & 0 & 0 & 0 \end{bmatrix}. \tag{4.8}$$

With the help of these matrices the decoupling control torque becomes:

$$\boldsymbol{\tau}_{dcp} = \boldsymbol{M}^*(\boldsymbol{q})\ddot{\boldsymbol{q}}_{pre} + \boldsymbol{C}^*(\boldsymbol{q}, \dot{\boldsymbol{q}})\dot{\boldsymbol{q}}, \tag{4.9}$$

where $\ddot{\boldsymbol{q}}_{pre}$ denotes the previous joint acceleration. This decoupling control torque is used as a feedforward control component.

Reconstruction of the gravity environment

We reconstruct the gravity environment for the pitch motion because the gravity environment is changed by the roll motion and the knee motion of the swing leg. The respective control torque cancels the coupling between Joints 2, 3 and Joints 1, 4. The motion is calculated with the gravity term of the equation of motion $\boldsymbol{g}(\boldsymbol{q})$. The control torque for reconstruction of the gravity environment for the pitch motion becomes:

$$\boldsymbol{\tau}_g = \boldsymbol{g}(\boldsymbol{q}) - \hat{\boldsymbol{g}}(\hat{\boldsymbol{q}}), \tag{4.10}$$

where $\hat{\boldsymbol{g}}(\hat{\boldsymbol{q}})$ denotes the gravity term of the virtual biped model.

Reference trajectory of the knee joint of the swing leg

We control the knee joint of the swing leg (Joint 4) with a given reference trajectory. The trajectory is generated by a time variant-function. The

reference trajectory for the knee joint of the swing leg q_{4d} is generated by a cubic sine function:

$$q_{4d}(t) = \begin{cases} A\sin^3(\frac{\pi}{t_{f4}}t) & (t \leq t_{f4}) \\ 0 & (t > t_{f4}), \end{cases} \tag{4.11}$$

where A denotes the amplitude of knee motion, t_{f4} denotes the final time and t is time. The trajectory has no energy dissipation due to collision of the knee joint. Consequently, the control torque for the knee joint becomes:

$$\boldsymbol{\tau}_{knee} = \begin{bmatrix} \mathbf{0} \\ \hline k_{p4}(q_{4d} - q_4) + k_{d4}(\dot{q}_{4d} - \dot{q}_{4d}) \end{bmatrix}, \tag{4.12}$$

where k_{p4} and k_{d4} are positive feedback gains.

Synchronization between motions

3D walking needs synchronization between the motions in each of the two planes. The hip joint of the robot is locked at a specified timing for synchronization between the pitch and the roll motion. Specifically, we lock the joint when the velocity of the hip joint becomes zero: $\dot{q}_3 = 0$. The hip locking torque is derived from the Lagrange multiplier with constraint $\ddot{q}_3 = 0$:

$$\boldsymbol{\tau}_{lock} = \boldsymbol{J}^T\lambda, \tag{4.13}$$

where

$$\boldsymbol{J} = \begin{bmatrix} 0 & 0 & 1 \end{bmatrix}, \tag{4.14}$$

$$\lambda = -\{\boldsymbol{J}\{\boldsymbol{M}(\boldsymbol{q})\}^{-1}\boldsymbol{J}^T\}^{-1} \{\boldsymbol{J}\{\boldsymbol{M}(\boldsymbol{q})\}^{-1}(\boldsymbol{\tau} - \boldsymbol{C}(\boldsymbol{q}, \dot{\boldsymbol{q}})\dot{\boldsymbol{q}} - \boldsymbol{g}(\boldsymbol{q}))\}. \tag{4.15}$$

Because of the chosen lock timing, it is easy to synchronize the roll and the pitch motions.

Roll motion stabilization

In the past, we examined the performance under the two different roll motion control methods and respective reference trajectories [13].

The first method is PD control of the ankle roll joint with a given reference trajectory which is generated by a spline function. The main point of the first method is to determine the initial and the final values by analysis of the collision equation. It is known that limit cycle based walking patterns are generally periodic. Therefore, we can obtain post-collision states for stable walking by analyzing the equation of collision and the kinematics of the robot as shown in the following equations:

$$\begin{aligned} \boldsymbol{q}_{fin} &= \boldsymbol{q}^- \\ &= \begin{bmatrix} q_1^+ \\ q_2^+ + q_3^+ \\ -q_3^+ \\ 0 \end{bmatrix} \end{aligned} \tag{4.16}$$

$$\begin{aligned} \dot{\boldsymbol{q}}_{fin} &= \dot{\boldsymbol{q}}^- \\ &= \{\boldsymbol{Q}^-(\boldsymbol{q}^-)\}^{-1}\boldsymbol{Q}^+(\boldsymbol{q}^+)\dot{\boldsymbol{q}}^+, \end{aligned} \tag{4.17}$$

where $\boldsymbol{q}_{fin}$ is pre-collision state. The reference trajectory generated via the spline function satisfies the states which are obtained by this analysis.

On the other hand, the second method is quite an empirical one. The control method for the ankle roll joint is tracking control with an empirical reference trajectory based on the relation between the CoM position and the mechanical energy. The reason why we choose this relation is to imitate energy feedback control because the reference trajectory of energy feedback control is in fact a relation between the CoM position and the mechanical energy which includes the frontal plane velocity only. The reference trajectory is empirical, therefore, it is difficult to explain why we can obtain a

trajectory for the relation between the CoM position r_{Cx} and the mechanical energy of the frontal plane $E_f = \frac{1}{2} m_{tot} r_{Cy}^2$ which includes the frontal plane velocity r_{Cy} only. In simple terms, we did the following tasks:

1. we repeated the simulation which limits the motion to the frontal plane with reasonable flat torque of the ankle roll joint a number of times;
2. we checked the input torque and the trajectory of the CoM position;
3. we generated a reference trajectory of the mechanical energy based on the better results of the simulations. Note that we defined the better results as the trajectory with small joint torque;
4. we applied the reference trajectory to the 3D biped simulation and we adjusted the trajectory accordingly.

The CoM in the frontal plane trajectory is:

$$\begin{aligned} E_{d-f}(r_{Cx}) &= -11926 r_{Cx}^6 - 2087.1 r_{Cx}^5 + 657.95 r_{Cx}^4 && (4.18) \\ &\quad +151.42 r_{Cx}^3 + 46.79 r_{Cx}^2 \\ &\quad -0.5337 r_{Cx} - 0.0024. && (4.19) \end{aligned}$$

Consequently, the second control method (the empirical method) for the ankle roll joint is:

$$\boldsymbol{\tau}_{emp} = \begin{bmatrix} k\{E_{d-f}(r_{Cx}) - E_f\} \\ 0 \\ 0 \end{bmatrix}, \qquad (4.20)$$

where k is a constant positive feedback gain.

In the past, we examined their performances. As the result, we concluded that the roll motion control with the empirical reference trajectory is superior to that with the spline reference trajectory, from view point of energy efficiency. However, it isn't clear how to generate the reference trajectory

because the reference trajectory generation depends on the experience of the researchers.

This section uses the control method for the ankle roll joint, which is tracking control with an empirical reference trajectory $\boldsymbol{\tau}_{emp}$.

4.2.3 Numerical simulation

Figure 4.6 shows the simulation results of Limit Cycle Walking with the above control method where $\phi = 0.04$ rad, $\zeta = 100.0t + 5.0$ s^{-1}, $\mu = -6.0$, $A = 0.4$ m, $t_{f4} = 0.7$ s, $k_{p4} = 100$ Nm/rad, $k_{d4} = 10$ Nms/rad and $k = 3000$ Nm/rad. Figure 4.6 (a) is the appearance of the walking locomotion, Figure 4.6 (b) is the phase portrait. The walking pattern is periodical. However, according to Fig. 4.6 (c), the ankle pitch joint (Joint 2) needs very large torque. As the cause of this result, we can consider the coupling between knee joint control and energy feedback control.

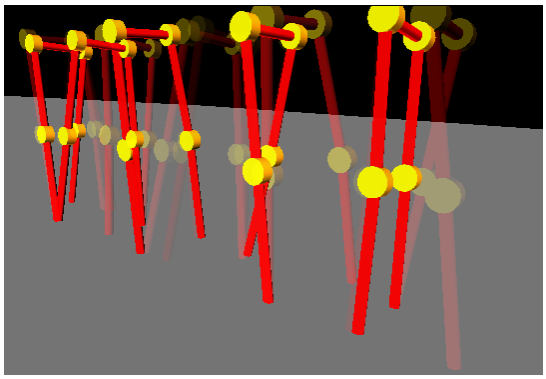

(a)

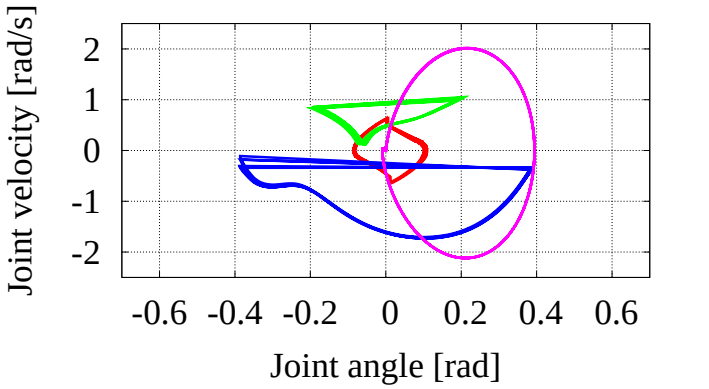

(b)

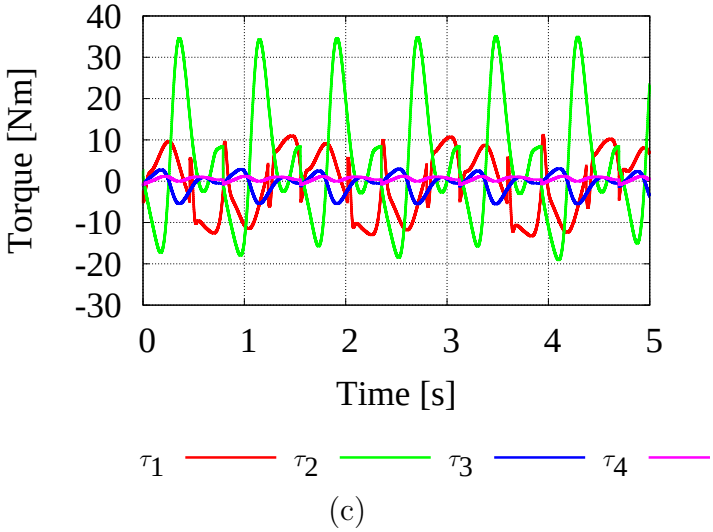

(c)

Fig. 4.6: Simulation results of the Limit Cycle Walking of the biped model with knee joint: (a) behavior of walking locomotion, (b) phase portrait, (c) control torque.

4.3 Seven DOF Biped Model

As described in Section 3.2, the upper body is very important for humanoid robots. Hence, this section considers 3D walking pattern generation for a biped model with an upper body.

4.3.1 Biped model

This section deals with a 7DOF 3D biped model as shown in Fig. 4.7. The physical parameters of the biped model are shown in Table 4.2. The model is composed of seven joints and seven links, including two legs and a torso. Each leg consists of a foot, a shank and a thigh. The seven joints are the ankle joints with 2DOF each, the knee joint of the swing leg with 1DOF and the 1DOF revolute joint for the upper body pitch motion. We assume the support leg to be always fixed to the ground. We also assume that link inertia moment and joint friction can be ignored. The generalized coordinates of the model are the joint angles: $\boldsymbol{q} = \begin{bmatrix} q_1 & q_2 & q_3 & q_4 & q_5 & q_6 & q_7 \end{bmatrix}^T$, while the generalized force vector is represented in terms of joint torque as $\boldsymbol{\tau} = \begin{bmatrix} \tau_1 & \tau_2 & \tau_3 & \tau_4 & \tau_5 & \tau_6 & \tau_7 \end{bmatrix}^T$. The biped is modeled as a hybrid dynamical system with two phases: the support phase, modeled with the motion equation, and the leg switch phase, modeled with the impact dynamics equation. It is assumed that leg switching occurs instantaneously.

4.3.2 Walking generation and control

The control for this model is combination method of energy feedback control with virtual biped model for the 2D biped model with upper body as described in Section 3.2 and decoupling control which is dealt with in Section 4.2.

The control for stabilizing pitch motion in the sagittal plane is similar to Section 4.2. The decoupling control torque is calculated with the matrices

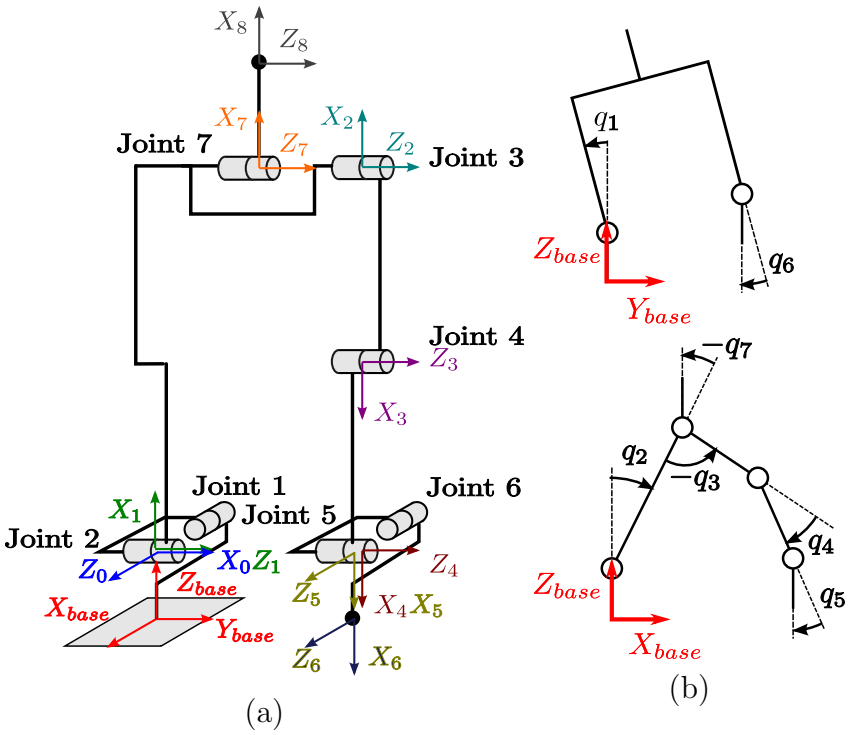

Fig. 4.7: 7DOF 3D biped model.

$\boldsymbol{M}(\boldsymbol{q})$ and $\boldsymbol{C}(\boldsymbol{q}, \dot{\boldsymbol{q}})$ which are included in the motion equation:

$$\boldsymbol{M}(\boldsymbol{q}) = \begin{bmatrix} M_{11} & \cdots & M_{17} \\ \vdots & \ddots & \vdots \\ M_{71} & \cdots & M_{77} \end{bmatrix}, \tag{4.21}$$

$$\boldsymbol{C}(\boldsymbol{q}, \dot{\boldsymbol{q}}) = \begin{bmatrix} C_{11} & \cdots & C_{17} \\ \vdots & \ddots & \vdots \\ C_{71} & \cdots & C_{77} \end{bmatrix}. \tag{4.22}$$

The second to the fifth and the seventh rows of the equation of motion describe the moments on the pitch joints (Joints 2, 3, 4, 5, 7). The first and the sixth columns of these two rows describe the coupling moment due to the roll joints (Joints 1, 6). Therefore, the matrices for decoupling control

Table 4.2: Physical parameters of the 7DOF 3D biped model.

Link name	Mass [kg]
Upper body	$m_b = 10.0$
Thigh	$m_t = 2.5$
Shank	$m_s = 2.5$
Foot	$m_f = 1.0$
Link name	**Length [m]**
Upper body	$l_b = 0.5$
Thigh	$l_t = 0.5$
Shank	$l_s = 0.5$
Foot	$l_f = 0.2$
Pelvis	$l_p = 0.3$

become:

$$\boldsymbol{M}^*(\boldsymbol{q}) = \begin{bmatrix} 0 & M_{12} & M_{13} & M_{14} & M_{15} & 0 & M_{17} \\ M_{21} & 0 & \cdots & \cdots & 0 & M_{26} & 0 \\ M_{31} & \vdots & \ddots & & \vdots & M_{36} & \vdots \\ M_{41} & \vdots & & \ddots & \vdots & M_{46} & \vdots \\ M_{51} & 0 & \cdots & \cdots & 0 & M_{56} & 0 \\ 0 & M_{62} & M_{63} & M_{64} & M_{65} & 0 & M_{67} \\ M_{71} & 0 & \cdots & \cdots & 0 & M_{76} & 0 \end{bmatrix}, \tag{4.23}$$

$$\boldsymbol{C}^*(\boldsymbol{q}, \dot{\boldsymbol{q}}) = \begin{bmatrix} 0 & C_{12} & C_{13} & C_{14} & C_{15} & 0 & C_{17} \\ C_{21} & 0 & \cdots & \cdots & 0 & C_{26} & 0 \\ C_{31} & \vdots & \ddots & & \vdots & C_{36} & \vdots \\ C_{41} & \vdots & & \ddots & \vdots & C_{46} & \vdots \\ C_{51} & 0 & \cdots & \cdots & 0 & C_{56} & 0 \\ 0 & C_{62} & C_{63} & C_{64} & C_{65} & 0 & C_{67} \\ C_{71} & 0 & \cdots & \cdots & 0 & C_{76} & 0 \end{bmatrix}. \tag{4.24}$$

With the help of these matrices the decoupling control torque becomes:

$$\boldsymbol{\tau}_{dcp} = \boldsymbol{M}^*(\boldsymbol{q})\ddot{\boldsymbol{q}}^* + \boldsymbol{C}^*(\boldsymbol{q}, \dot{\boldsymbol{q}})\dot{\boldsymbol{q}}, \tag{4.25}$$

where $\ddot{\boldsymbol{q}}^*$ denotes the joint acceleration vector of the previous sampling time. This decoupling control torque is used as a feedforward control component.

We also apply reconstruction of the gravity environment. The control torque which cancels the influence of the roll motion is calculated with the gravity term of the equation of motion $\boldsymbol{g}(\boldsymbol{q})$.

$$\boldsymbol{\tau}_g = \boldsymbol{g}(\boldsymbol{q}) - \hat{\boldsymbol{g}}(\hat{\boldsymbol{q}}), \tag{4.26}$$

where $\hat{\boldsymbol{g}}(\hat{\boldsymbol{q}})$ denotes the gravity term of the virtual biped model.

Besides, the constraint for synchronization between pitch and roll motion is similar to Section 4.2. In addition, in order to the foot of the swing leg conserves the parallel orientation to the floor consistently, the ankle roll joint of the swing leg is controlled as Eq. 3.22.

4.3.3 Numerical simulation

Figure 4.8 shows the numerical simulation results. In this simulation, for stabilizing the motion in the frontal plane, we use the tracking control of the ankle roll joint with a given reference trajectory generated via a spline function (see Section 4.2).

Figure 4.8 (a) shows the phase portrait. From this figure, we can see that the biped model can walk stably. On the other hand, from Fig. 4.8 (b), it is seen that τ_1 (joint torque of ankle roll joint) and τ_2 (joint torque of ankle pitch joint) are excessive. We think that the ankle roll joint needs a large control torque because the reference trajectory generated via the spline function is not suitable from view point of energy efficiency. We also think that the control torque of the ankle pitch joint is excessive because the energy feedback control with the virtual biped model and the knee joint PD control interfere.

As a result, we can conclude that we have to consider generation of a suitable reference trajectory for roll motion, from view point of energy effi-

ciency without any empirical methods. Besides, we also have to design the extended feedback control for stabilizing motion in the sagittal plane because the control methods shouldn't interfere.

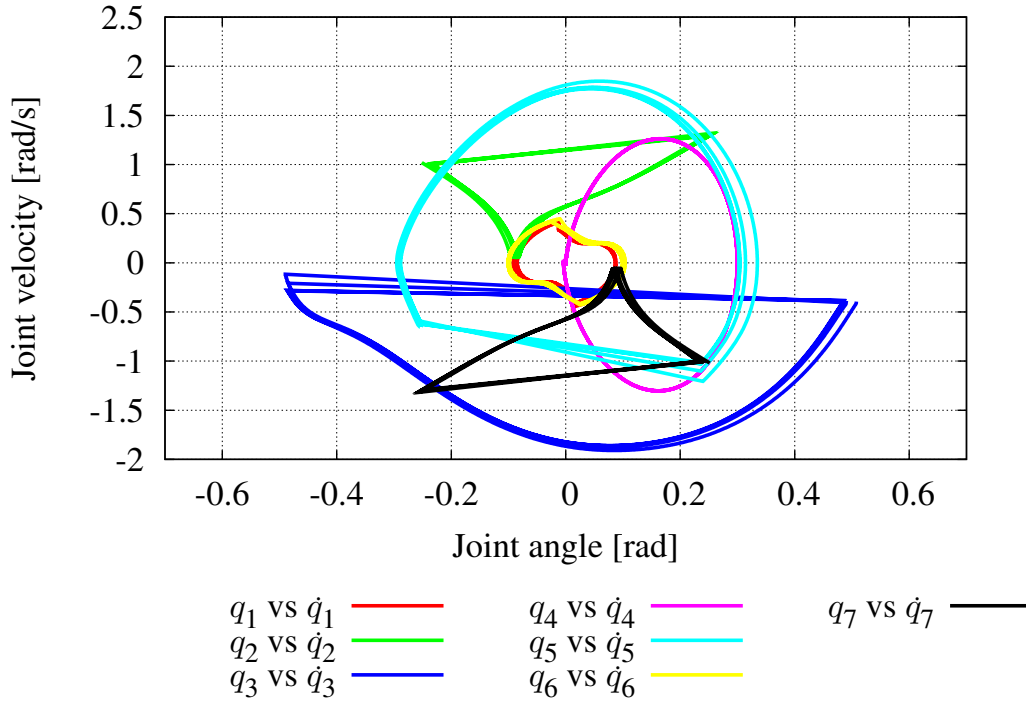

(a)

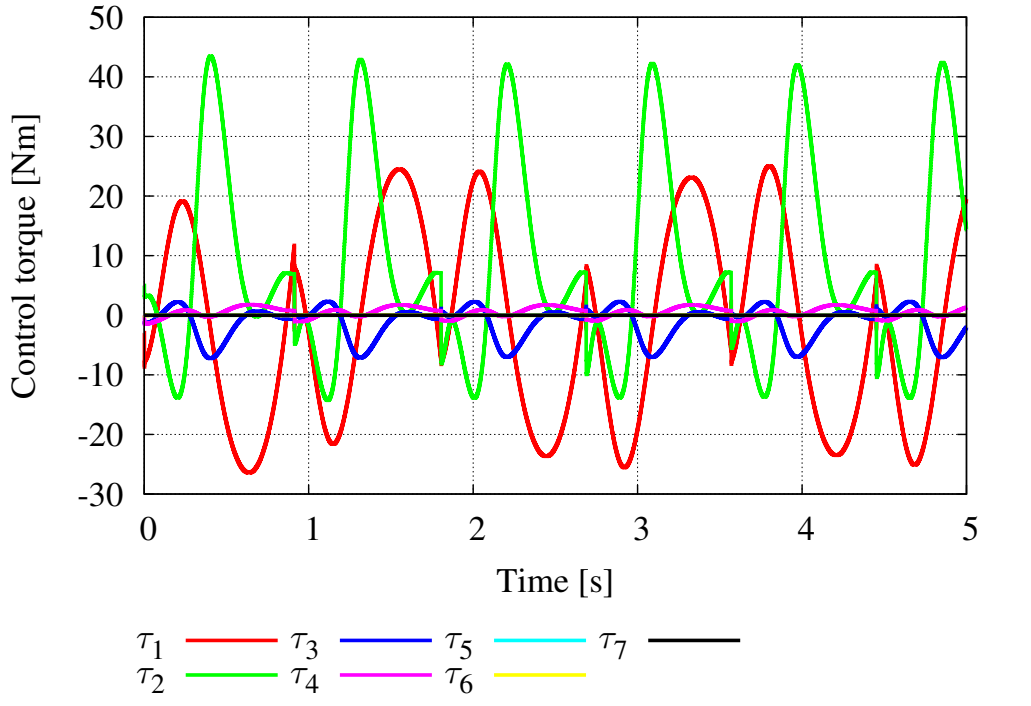

(b)

Fig. 4.8: Simulation results of the Limit Cycle Walking of the 3D 7DOF biped model: (a) phase portrait, (b) control torque ($\boldsymbol{\tau}_{dcp} + \boldsymbol{\tau}_g + \boldsymbol{\tau}_{ef} + \boldsymbol{\tau}_{roll}$).

4.4 Extended Energy Feedback Control

Originally, with energy feedback control, stable walking of the compass biped model can be realized based on the PDW concept. We apply this control method to complex biped models. Therefore, in this subsection, we propose an extended energy feedback control.

Based on Eq. 2.19, the control torque of the energy feedback control is in general expressed by the following equation:

$$\boldsymbol{\tau}_{eef} = \boldsymbol{\mu} \frac{m_{tot} g \dot{r}_{Cx} \tan\phi - \zeta(E - E_d(r_{Cx}))}{\boldsymbol{\mu}^T \dot{\boldsymbol{q}}}, \tag{4.27}$$

where $\boldsymbol{\mu}$ denotes the torque ratio vector between all joints. From Eq. 4.27, we can see that $\boldsymbol{\mu}$ determines the input energy based on the PDW concept to the joints. Therefore, the setting of a suitable $\boldsymbol{\mu}$ is very important to generate stable walking. In Chapter 2, we could derive μ which is constant from the torque ratio of VPDW of the compass biped model (see Eq. 2.18) because the control torque of VPDW of that model is flat during the single support phase. However, from Fig. 3.8, we can see that the joint torque of VPDW of the biped model with upper body, ankle and knee isn't flat, because the knee joint is controlled by PID control (see Eq. 3.11). Therefore, it is not easy to determine a suitable $\boldsymbol{\mu}$.

4.4.1 2D Virtual Passive Dynamic Walking with knee joint control based on virtual gravity

In order to obtain a suitable $\boldsymbol{\mu}$ for stable walking, in this subsection, we derive the control torque ratio from VPDW by using virtual gravity based knee joint control.

Here we deal with the 2D biped model as shown in Fig 3.7. Control torque based on the VPDW is derived from Eq. 2.7. The control torque for the knee joint is derived from virtual gravity. Besides, the constraints of the

upper body and the ankle joint of the swing leg are the same as that of Subsection 3.2.1. VPDW by using virtual gravity based knee joint control needs to lock the knee of the swing leg when the swing leg's knee joint becomes straight. In this paper, we constraint the knee joint of the swing leg using the Lagrange multiplier method.

Figure 4.9 shows the simulation results of VPDW by using knee joint control based on virtual gravity, where $\phi = 0.02$ rad. Figure 4.9 (a) shows that the control torques for VPDW of the biped model is flat. This feature is similar to PDW of the compass biped model (see Fig. 2.5 (a)). In addition, we can see that the mechanical energy increases monotonically during the single support phase as shown in Fig.4.9 (b) except one discontinuous energy jump. From this result, we can see that the knee joint locking causes the mechanical energy to dissipate. This feature isn't similar to that with the VPDW with PID knee joint control with the reference trajectory generated by by a cubic sine function (see Fig. 3.8 (b)). From the phase portrait (Fig.4.9 (c)), we can see that the biped model can indeed walk stably and periodically. Consequently, we can achieve flat control torque typical for stable walking. Therefore, the control torque ratio vector $\boldsymbol{\mu}$ is obtained in a similar way as the control torque ratio μ in Section 2.4. However, when the knee is controlled by virtual gravity force only, the *foot-scuffing* problem may occur. The problem and solution is described in Appendix B.

4.4.2 Biped walking of 2D biped model based on extended energy feedback control

In the last subsection, we have shown how to obtain the control torque ratio $\boldsymbol{\mu}$. Therefore, in this subsection, we apply the extended energy feedback control to the 2D biped model as shown Fig 3.7. The control torque can be calculated from Eq. 4.27. However, as shown in Fig. 4.9 (b), this walking pattern has energy dissipation because of the knee joint locking. Hence, the

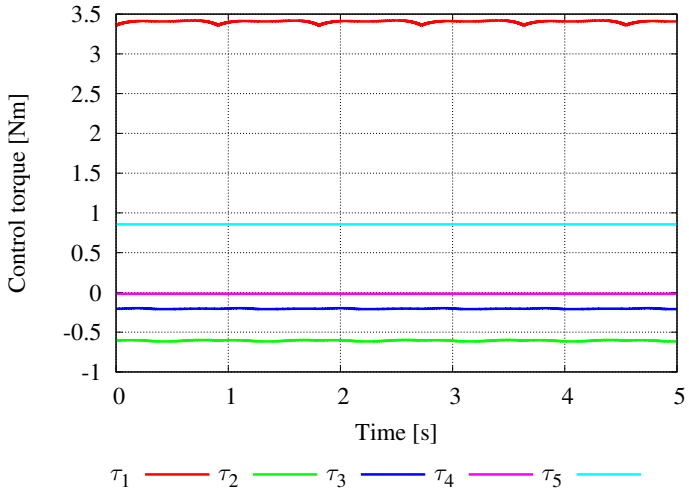

(a)

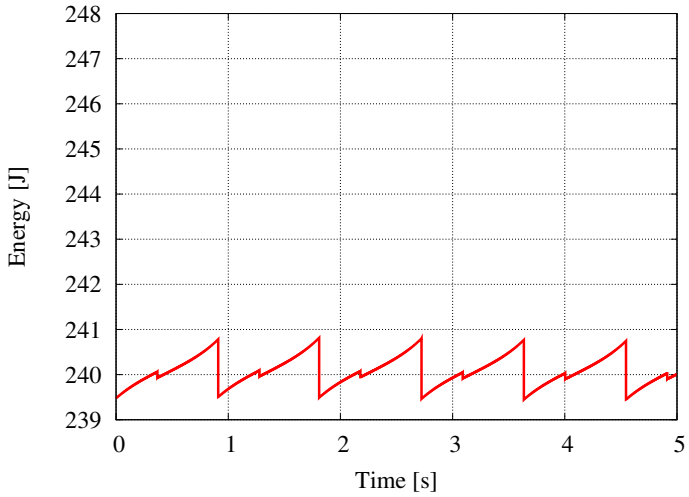

(b)

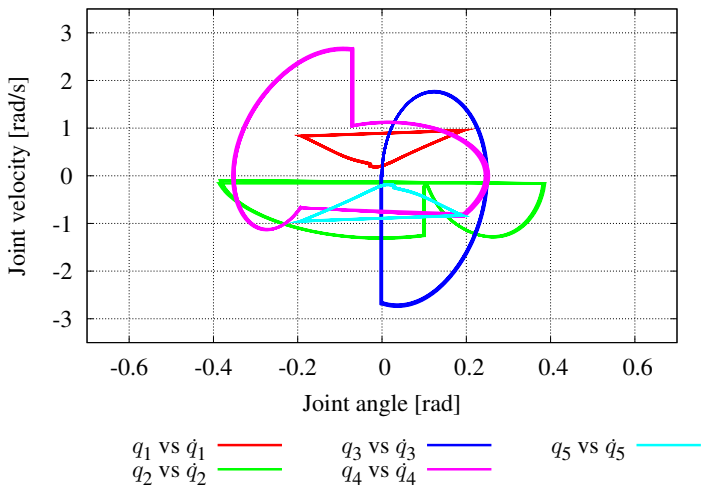

(c)

Fig. 4.9: Simulation results of the VPDW by using knee joint control based on virtual gravity: (a) control torque for VPDW, (b) mechanical energy, (c) phase portrait.

desired mechanical energy $E_d(r_{Cx})$ is derived from the following equation:

$$E_d(r_{Cx}) = m_{tot} g r_{Cx} \tan\phi + E_0 + E_{loss}, \tag{4.28}$$

where E_{loss} denotes the mechanical energy loss of the knee joint locking. Before locking of the knee joint, $E_{loss} = 0$ but, after the knee joint locking, E_{loss} can be calculated as:

$$E_{loss} = E^+ - E^-, \tag{4.29}$$

where E^- and E^+ denote pre- and post-locking mechanical energies, respectively.

Figures 4.10 and 4.11 show the simulation results of the limit cycle based walking based on the extended energy feedback control, where $\phi = 0.013$ rad, $\boldsymbol{\mu} = \begin{bmatrix} 1 & -0.18 & -0.06 & 0 & 0.25 \end{bmatrix}^T$, $\zeta = 10$ s^{-1} and $E_0 = 240$ J. From Fig. 4.10, we can see that it is possible to generate quite periodic walking pattern by using extended energy feedback control. Figure 4.11 gives the simulation results when motion starts from an unsuitable initial state. The initial state is in the neighborhood of the stable equilibrium point. It is possible to see that the mechanical energy is stabilized asymptotically to the desired energy trajectory by energy feedback control.

4.4.3 Biped walking of 3D biped model based on extended energy feedback control

In this subsection, we generate limit cycle based walking of the 3D biped model. This subsection deals with the 3D biped model shown in Fig. 4.7. The physical parameters of the biped model and assumptions of numerical simulation are same as those in Section 4.3.

In this subsection, we propose an improved combination control method. The control is decoupling control in combination with reconstruction of the

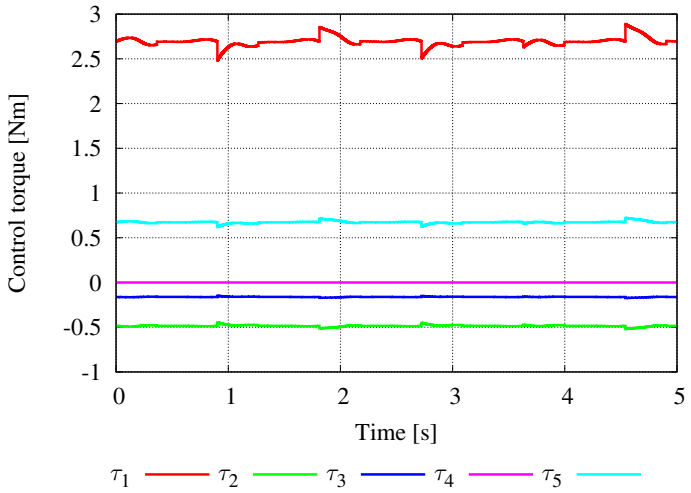

(a)

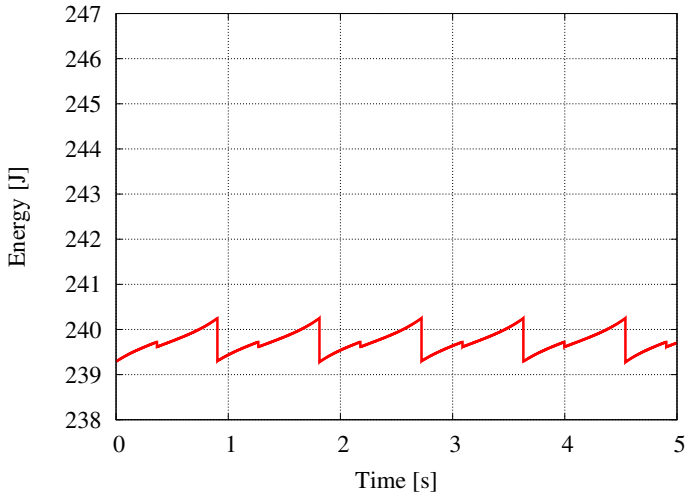

(b)

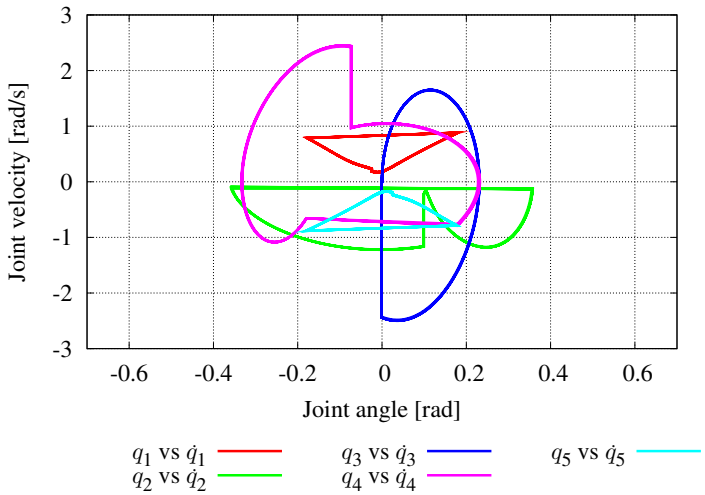

(c)

Fig. 4.10: Simulation results of the extended energy feedback control: (a) control torque for extended energy feedback control, (b) mechanical energy, (c) phase portrait.

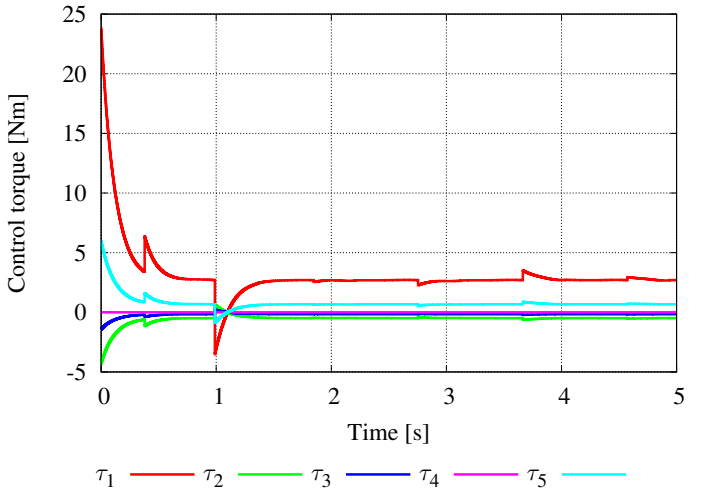

(a)

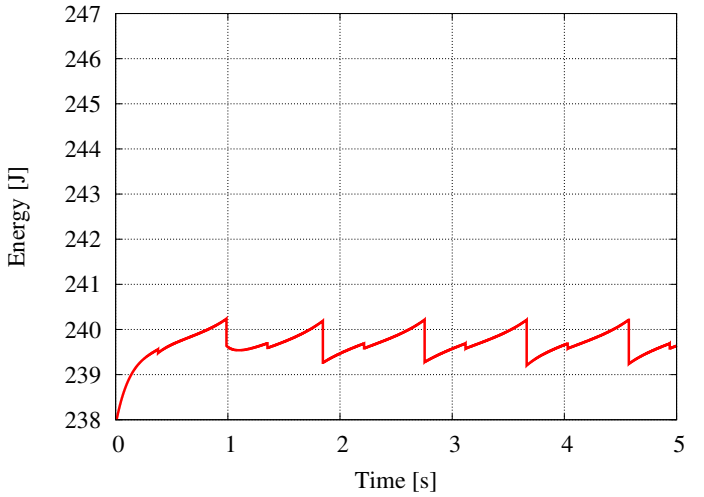

(b)

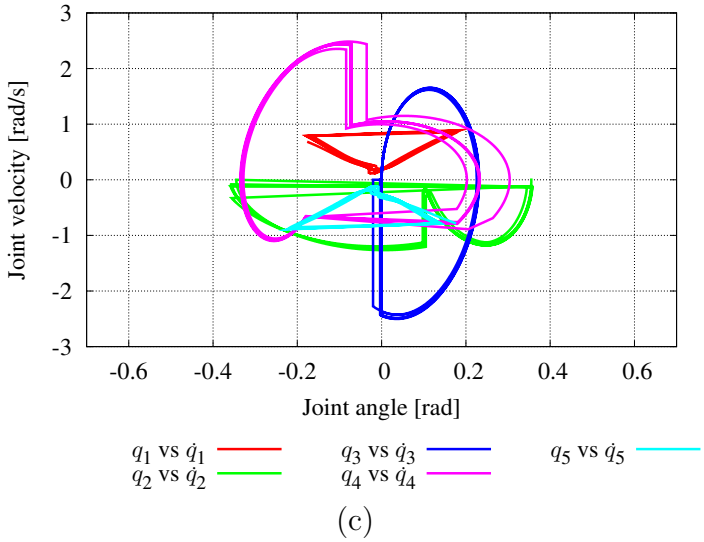

(c)

Fig. 4.11: Simulation results of the extended energy feedback control which starts walking from the neighborhood of the stable equilibrium point: (a) control torque for extended energy feedback control, (b) mechanical energy, (c) phase portrait.

gravity environment which were dealt with in Section 4.3 plus extended energy feedback control for stabilizing the motion in the sagittal plane. The control torque is derived from the following equation:

$$\boldsymbol{\tau} = \boldsymbol{\tau}_{dcp} + \boldsymbol{\tau}_g + \boldsymbol{\tau}_{eef} + \boldsymbol{\tau}_{roll} + \boldsymbol{J}_M^T \boldsymbol{\lambda}_C, \tag{4.30}$$

$\boldsymbol{\tau}_{dcp}$ denotes the joint torque for decoupling control which can be computed from $\boldsymbol{M}(\boldsymbol{q})$ and $\boldsymbol{C}(\boldsymbol{q}, \dot{\boldsymbol{q}})$, which are included in the equation of motion, $\boldsymbol{\tau}_g$ denotes the joint torque for reconstruction of the gravity environment, $\boldsymbol{\tau}_{eef}$ denotes the torque for extended energy feedback control, $\boldsymbol{\tau}_{roll}$ denotes the control torque for stabilizing the motion in the frontal plane and $\boldsymbol{J}_M^T \boldsymbol{\lambda}_C$ denotes the torque for the constraints. The constraints include the hip locking torque for synchronization between the motions in the frontal and sagittal planes, the locking torque of the knee joint of the swing leg, and the control torque of the ankle joint of the swing leg and the upper body. In this control, unlike previous combination control which was proposed in Section 4.2, 4.3, extended energy feedback control includes knee joint control torque.

Figures 4.12 and Fig. 4.13 are the numerical simulation results of the 3D limit cycle based walking. Figure 4.12 shows the results, where the energy feedback control gain $\zeta = 50$ s^{-1}. Figure 4.12 (a) shows the phase portrait. From this figure, we can see that the biped model can walk stably. On the other hand, from Fig. 4.12 (b), we can see that joint torque of the ankle pitch joint τ_2 is smaller than that of Fig. 4.8 (b). However, at the post-collision between the foot of the swing leg and the floor, the ankle pitch joint requires excessive torque. We think that the ankle pitch joint needs a large control torque instantaneously because the pre-collision state, which is achieved via the analysis of the collision equation, is not optimal. Therefore, it is necessary to adjust the energy feedback gain ζ. Figure 4.13 shows the results, where the energy feedback control gain is $\zeta = 100t$ s^{-1} (t is the time) used to avoid excessive joint torque. From Fig. 4.13 (b), we can see that the control torque of the ankle pitch joint is decreased by adjustment of ζ.

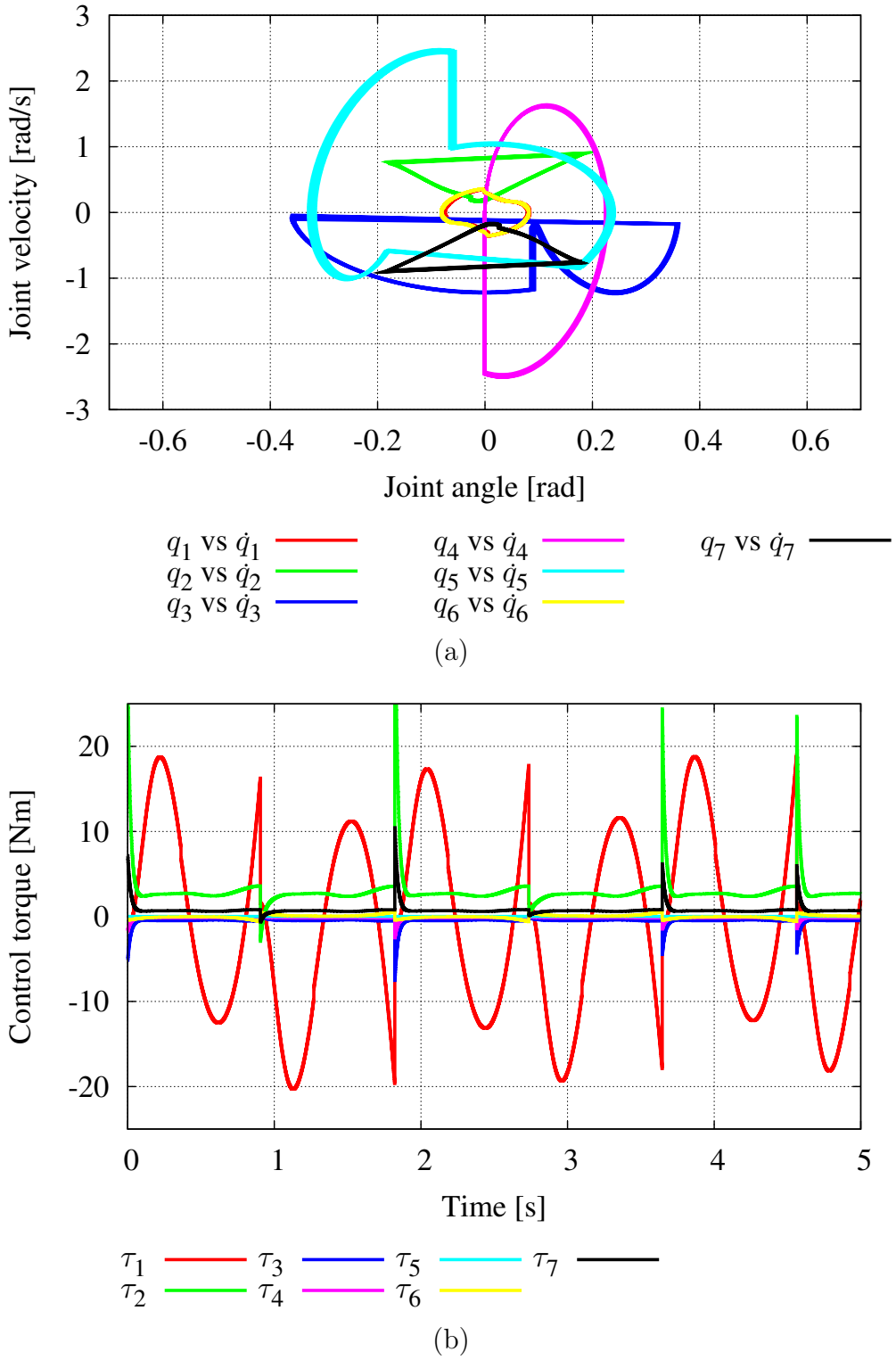

Fig. 4.12: Simulation results of the Limit Cycle Walking of the 3D 7DOF biped model based on improved combination control (1): (a) phase portrait, (b) control torque ($\boldsymbol{\tau}_{dcp} + \boldsymbol{\tau}_g + \boldsymbol{\tau}_{eef} + \boldsymbol{\tau}_{roll}$).

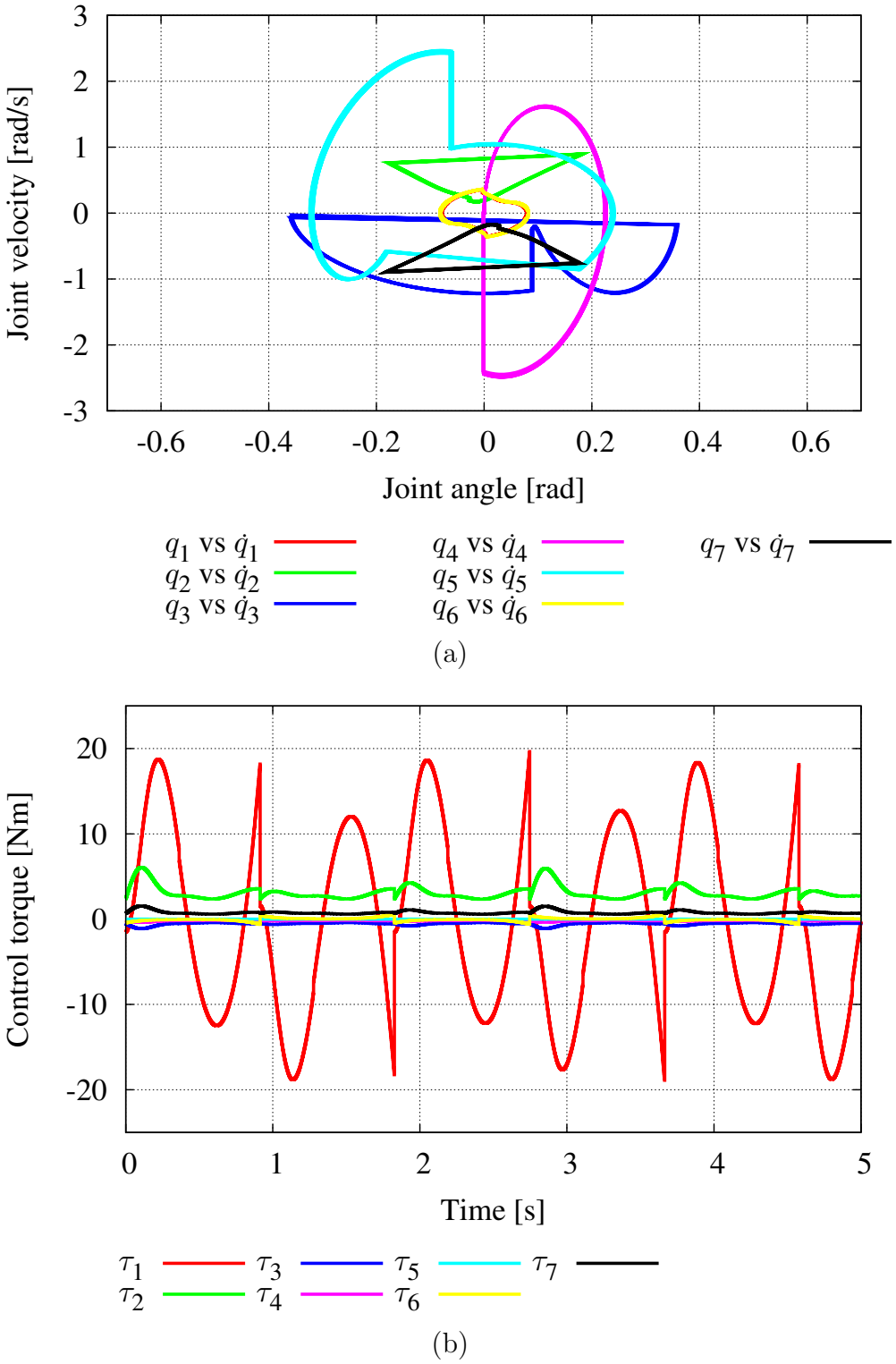

Fig. 4.13: Simulation results of the Limit Cycle Walking of the 3D 7DOF biped model based on improved combination control (2): (a) phase portrait, (b) control torque ($\boldsymbol{\tau}_{dcp} + \boldsymbol{\tau}_g + \boldsymbol{\tau}_{eef} + \boldsymbol{\tau}_{roll}$).

4.5 Discussion and Conclusions

In this chapter, we dealt with two 3D biped models. We generated walking patterns respectively and we showed that the biped models can walk stably with our control methods. Consequently, we solved the problems of 3D limit cycle based walking as described in Section 4.1, with proper control torques. 3D walking based on a limit cycle is impossible because there isn't any energy input for roll motion in the frontal plane. Therefore, it is necessary to stabilize roll motion by some joint torques or some special mechanism. The features of our control are:

- our biped model doesn't need special mechanisms for stabilizing roll motion (e.g. semi circular feet);
- we generate the 3D walking pattern based on the limit cycle of the 2D simple biped model.

It is known that semicircular feet are effective for energy efficiency. However, flat feet are more versatile than curved feet. Humanoid robots are required to perform many kinds of tasks. Hence we think that versatility is important for humanoid robots. It is difficult to find a stable limit cycle of the biped model which has many DOF. We expect that our method based on limit cycle of the simple biped model will enable us to generate a stable 3D walking pattern more easily than ever before.

We could generate the stable walking patterns for each model with the combination of energy feedback control for sagittal plane motion and tracking control for roll motion, etc. However, as the results show, our combined control is still far from practical application, because this control has some problems. Two important problems are described below. First, it isn't clear how to generate the reference trajectory of the motion in the frontal plane. Second, the controls interfere with each other. We think that the second problem is especially critical.

Therefore, recently we tried to developed a control method of motion in the sagittal plane. The control was designed based on the energy feature of Passive Dynamic Walking. The main point of enhancing of energy feedback control was how to determine the joint control ratio vector $\boldsymbol{\mu}$. In this Chapter, we derived $\boldsymbol{\mu}$ from 2D VPDW with virtual gravity based knee joint control. And we designed an extended energy feedback control for the 2D biped model. We confirmed that extended energy feedback control can generate stable biped walking. In addition, we applied a combination method of extended energy feedback control and decoupling control to the 3D biped model. We showed that the combination method can generate 3D stable walking and the control torque for stable walking is less than that of the method used in Section 4.3. However, the suitable control gain and initial state for stable walking have to be set empirically.

Chapter 5

Discussion and Future Research Directions

5.1 Conclusions

The aim of our study is limit cycle based walking pattern generation for humanoid robots. We think that the goals of biped walking, which are energy efficiency and naturalness, can be achieved via the Limit Cycle Walking concept, because this concept is based on the dynamics of the robot and the environment. Therefore, we consider biped walking optimization by using dynamic stability from the view point of energy efficiency.

We have been focusing on PDW which is one type of Limit Cycle Walking. Pure PDW is generated by interaction between the dynamics of the robot and the environment. This biped walking requires only a shallow slope and a gravity force. Therefore, PDW was an ultimate level of energy efficiency. Hence, we are studying biped walking control methods based on the PDW concept which can be applied to humanoid robots.

However, Limit Cycle Walking like PDW has some inherent problems:

1. derivation of suitable initial condition to ensure a stable limit cycle;

2. only 2D compass biped model can walk, without control or a special

mechanism design;

3. lack of robustness, because PDW don't include any feedback control elements.

To achieve our aim, we have to solve these problems. We consider the first problem to be not any more so important, as it was impossible to be solved with the approach of analysis of dynamics. However, it is difficult to put this method into practical use, because nobody knows why a planar compass biped model can walk on a shallow slope. Consequently, we think that it is important to take full advantage of the fact from the viewpoint of engineering. For example, there is a memory-based control method that uses a database of walking patterns based on Limit Cycle Walking. Also, we consider that it is very important to pay attention to the dynamic parameters of the robot, at the stage of the design of the robot. There have been some researches of the relation between the dynamic parameters and Limit Cycle Walking by experiments and numerical simulations so far [16]-[18]. These researches are of the greatest assistance to design biped robots. However, humanoid robots need general versatility, for performing various tasks. Because humanoid robots are expected to assist us in varied situations. Hence, when designing the robot, we have to consider not only the performance of biped walking but also how to achieve versatility. For example, it is known that semicircular feet are more effective for energy efficiency than flat feet. However, flat feet are more versatile than curved feet. Therefore, this work deals with robot which has flat feet (see Fig.4.7). Also, there are some researches on biped robots with flat feet [19], [20].

About the other problems, we can solve them with technical methods such as useful machinery, and control methods. In this thesis, we focused mainly on the second problem. We can understand the fundamentals of PDW through the study of a compass biped model (see Chapter 2). On that ba-

sis, in Chapter 3, we designed controllers for extended 2D biped models (see Fig. 3.1, 3.7). We confirmed the performances of these controllers via numerical simulations. The most important components of the controllers are energy feedback and virtual biped model concept. Especially, we expect that virtual biped model concept enable us to generate stable walking patterns of complex biped models more easily than ever before. Energy feedback control can achieve PDW based feedback.

To achieve 3D Limit Cycle Walking, we have to consider yaw-to-pitch or roll-to-pitch coupling. As a possible approach, we have proposed a combination of decoupling control, energy feedback control and so on [13]. In Section 4.2, 4.3, we designed the combination controllers for the biped model with ankle and knee, and the biped model with ankle, knee and upper body based on virtual biped model concept. Firstly, we used energy feedback control based on the virtual biped model without knee joint for stabilization of the motion in the sagittal plane. The controllers could achieve 3D stable walking. However, the control torque of the ankle pitch joint is excessive because the energy feedback control with the virtual biped model with out knee and the knee joint PD control interfere. Therefore, in Section.4.4, we designed extended energy feedback control. The control torque ratio is very important to this controller. We obtained the ratio from VPDW with knee joint control based on virtual gravity. We confirmed effectiveness of extended energy feedback control via numerical simulations (see Fig. 4.10, 4.11). In addition, we applied the combination of extended energy feedback control, decoupling control and so on to 3D biped model with ankle, knee and upper body. We could see that the biped model can walk stably based on the controller.

Finally, we summarize the problems of 3D Limit Cycle Walking as follows:

- It is needed to optimize the reference trajectory of the ankle roll joint.

- It is necessary to determine the suitable parameters for the controller.
- We have to set a virtual biped model which is most appropriate to the actual robot.

5.2 Future Tasks

Our aim is to apply a high-efficient limit cycle based walking pattern to humanoid robots. However, there remains still much work to achieve the purpose. We have to:

- solve the inherent problem of suitable initial state by analysis of the robot;
- optimize 3D Limit Cycle Walking:
  - consider the reference trajectory of the ankle roll joint of the stance leg, the ankle and knee joint of the swing leg and upper body from view point of energy efficiency and stability;
  - consider how to determine the suitable parameters for the controller;
  - set a virtual biped model which is appropriate for the actual robot.
- consider yaw motion and sliding. One should pay attention to yaw-to-pitch coupling. We guess that coupling is quite large. Yaw motion is an obstacle to stable walking pattern generation within our present control approach;
- consider the double support phase. It is expected the phase is useful to manipulate the robot state, therefore we may be able to stabilize or manipulate the limit cycle of biped walking. In addition, the phase may be very important to match the controller given by numerical simulation to actual humanoid robots;

- prove stability of 3D Limit Cycle Walking based on our controller by Poincare map and so on;

- match the physical parameters and structure of biped model to that of actual humanoid robots, because the performance of Limit Cycle Walking is very sensitive to physical parameters. And then, we have to evaluate energy efficiency of the walking pattern generated based on our controller. We think that it is possible by comparison with that of conventional control method by using the cost of transport [7];

- step up the strictness of numerical simulation to match the actual world:

  - consider the environment, which includes a collision model between the foot of the swing leg and the ground, including elastic collision, friction and vibration. We guess that double support phase is very important to solve this issue.

We still have to solve a lot of problems. However, we expect that it is possible to achieve the goals of biped walking via researching of the Limit Cycle Walking concept.

Acknowledgment

The author is deeply grateful to Prof. Dragomir N. Nenchev and Dr. Daisuke Sato who provided carefully considered feedback and valuable comments. The author would also like to thank Mr. Naoyuki Hara and Takashi Miyasaka whose comments made enormous contribution to this research.

January, 29th 2010
Yuzuru Harada

References

[1] S. Kajita and T. Sugihara, "Humanoid robots in the future," *J. of the Robotics Society of Japan*, vol. 26, no. 7, pp. 761–762, 2008 (in Japanese).

[2] S. Kajita *et al.*, "Biped walking," in *Humanoid Robot*, Tokyo, Japan: Ohmsha, 2005, pp. 103–161 (in Japanese).

[3] T. Sugihara and Y. Nakamura, "High mobility control of humanoid robots based on an analogy of ZMP-CoG model and carted inverted pendulum model," *J. of the Robotics Society of Japan*, vol. 24, no. 1, pp. 74–86, 2006 (in Japanese).

[4] D. N. Nenchev *et al.*, "Motion feedback control at a singular configuration," *4th SICE System Integration Division Annual Conference (SI2003)*, Tokyo, Japan, 2003, pp. 508–509 (In Japanese).

[5] D. G. E. Hobbelen and M. Wisse, "Ankle actuation for limit cycle walkers," *The Int. J. of Robotics Research*, vol. 27, no. 6, pp. 709–735, 2008.

[6] T. McGeer, "Passive dynamic walking," *The Int. J. of Robotics Research*, vol. 9, no. 2, pp. 62–82, 1990.

[7] S. H. Collins *et al.*, "Efficient bipedal robots based on passive-dynamic walking," *Science*, vol. 307, pp. 1082–1085, 2005.

[8] A. Goswami *et al.*, "Limit cycles in a passive compass gait biped and passivity-mimicking control laws," *Autonomous Robots*, vol. 4, no. 3, pp. 273–286, 1997.

[9] F. Asano *et al.*, "Gait generation and Control for Biped Robots Based on Passive Dynamic Walking," *J. of the Robotics Society of Japan*, vol. 22, no. 1, pp. 130–139, 2004 (in Japanese).

[10] T. McGeer *et al.*, "Passive dynamic biped catalogue, 1991," in *Experimental Robotics II*, Toulouse, France: The 2nd International Symposium, 1991, pp. 465–490.

[11] M. Wisse *et al.*, "A 3D passive dynamic biped with yaw and roll compensation," *Robotica*, vol. 19, pp. 275–284, 2001.

[12] A. Kuo, "Stabilization of lateral motion in passive dynamic walking," *The Int. J. of Robotics Research*, vol. 18, no. 9, pp. 917–930, 1999 (In Japanese).

[13] K. Miyahara *et al.*, "Three-dimensional limit cycle walking with joint actuation," *in Proc. 2009 IEEE/RSJ Int. Conf. on Intelligent Robotics and Systems*, St. Louis, MO, USA, 2009, pp. 4445–4450.

[14] F. Asano *et al.*, "Biped gait generation and control based on a unified property of passive dynamic walking," *IEEE Trans. Robotics*, vol. 21, no. 4, pp. 754–762, 2005.

[15] H. Sasaki and M. Yamakita, "Efficient walking control of robot with torso based on passive dynamic walking," in *IEEE Int. Conf. on Mechatronics*, Kumamoto, Japan, 2007.

[16] F. Asano and Zhi-Wei Luo, "Underactuated virtual passive dynamic walking with an upper body," *Proc. of the IEEE Int. Conf. Robotics and Automation*, Pasadena, CA, USA, 2008, pp. 2441–2446.

[17] Y. Ikemata *et al.*, "A study of the leg-swing motion of passive walking," *Proc. of the IEEE Int. Conf. Robotics and Automation*, Pasadena, CA, USA, 2008, pp. 1588–1593.

[18] F. Asano and Zhi-Wei Luo, "Dynamics Walking Analyses of Underactuated Biped Robot That Added Upper Body by Means of Bisecting Hip Mechanism," *J. of the Robotics Society of Japan*, vol. 26, no. 8, pp. 932–943, 2008 (In Japanese).

[19] K. Narioka *et al.*, "3D Limit Cycle Walking of Musculoskeletal Humanoid Robot with Flat Feet," *in Proc. 2009 IEEE/RSJ Int. Conf. on Intelligent Robotics and Systems*, St. Louis, MO, USA, 2009, pp. 4676–4681.

[20] T. Kinugasa *et al.*, "3D Passive Walker with Ankle Spring and Flat Feet," *J. of the Robotics Society of Japan*, vol. 27, no. 10, pp. 1169–1172, 2009 (In Japanese).

[21] F. Asano and M. Yamakita, "Active Knee-Lock Algorithms and Virtual Coupling Control for Variable Walking Pattern of a Kneed Biped," *Transactions of the Institute of Systems, Control and Information Engineers*, vol. 14, no. 11, pp. 545–553, 2001.

Appendix A

Definitions of Planes and Axes

Generally, 3D motion is divided into planar motions for analysis or research. In this paper, we defined the frontal plane, the sagittal plane and the horizontal plane as shown in Fig. A.1. We also defined three axes which express

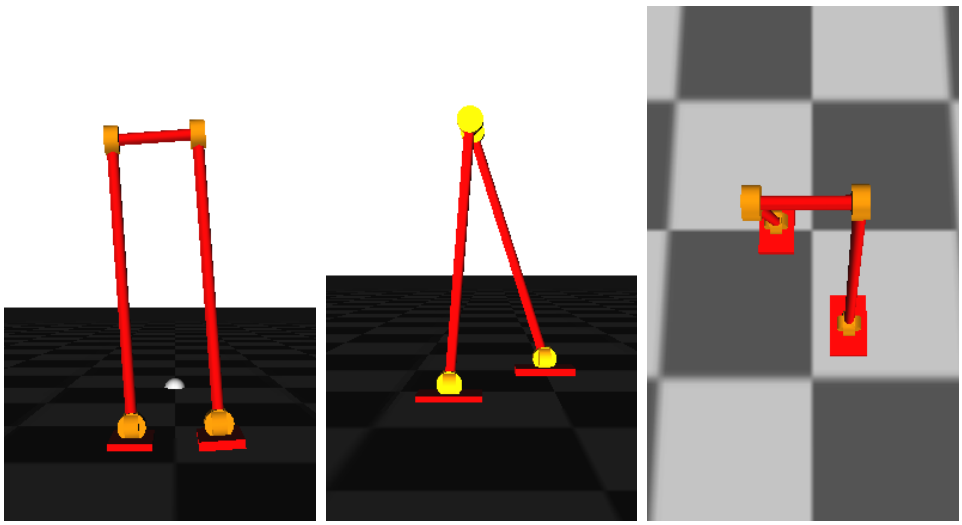

(a) (b) (c)

Fig. A.1: Definition of the planes: (a) frontal plane, (b) sagittal plane, (c) horizontal plane.

the motion direction as shown in Fig. A.2.

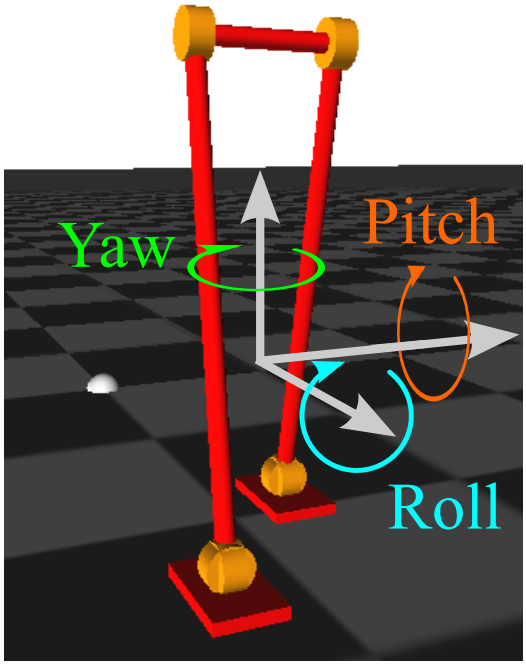

Fig. A.2: Definition of the axes.

Appendix B

Active Knee Lock Algorithm

In this chapter, we described the *foot-scuffing* problem. In order to obtain a suitable $\boldsymbol{\mu}$ for stable walking, in Section 4.4, we derive the control torque ratio from VPDW. If the biped model is controlled based on the most basic VPDW concept, the knee joint of the swing leg is controlled by virtual gravity force only. Then, the *foot-scuffing* problem may occur. Figure B.1 (a) shows the trajectory of the foot of the swing leg (the biped model is Fig. 3.7). From this figure, we can see that the foot scuffs the ground. To avoid the *foot-scuffing* without any other controls or special mechanisms, the shank of the biped model has to be more light than the thigh.

In order to solve the *foot-scuffing* problem, we can adopt two solutions. First solution is to use the motion in the frontal plane. Figure B.1 (b) shows the foot trajectory of 3D Limit Cycle Walking which is dealt with in Section 4.4. From this figure, we can see that the robot avoids *foot-scuffing* problem. On the other hand, second solution is active knee-lock algorithm. This algorithm is proposed by Asano *et al.* [21]. Firstly, the algorithm locks the knee joint when the joint velocity of the knee is 0 rad/s. Because, in that instant, mechanical energy dissipation by knee-lock becomes 0 J. And then, active knee lock is released at the arbitrary timing. This timing is very important because it determines the timing of stretching the knee.

Figure B.1 (c) shows the foot trajectory of 2D VPDW with active knee-lock. The biped model is Fig. 3.7). We set that the active knee lock is released when the angle of the hip joint $q_2 = -0.2$ rad. From this figure, we can see that the robot avoids *foot-scuffing* problem by active knee-lock algorithm.

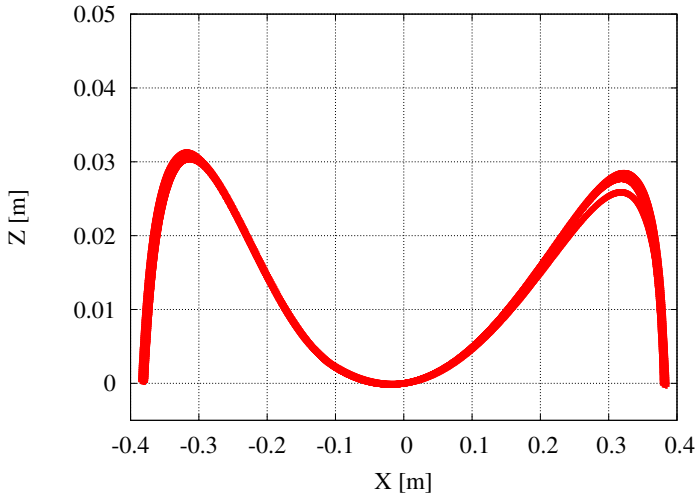

(a)

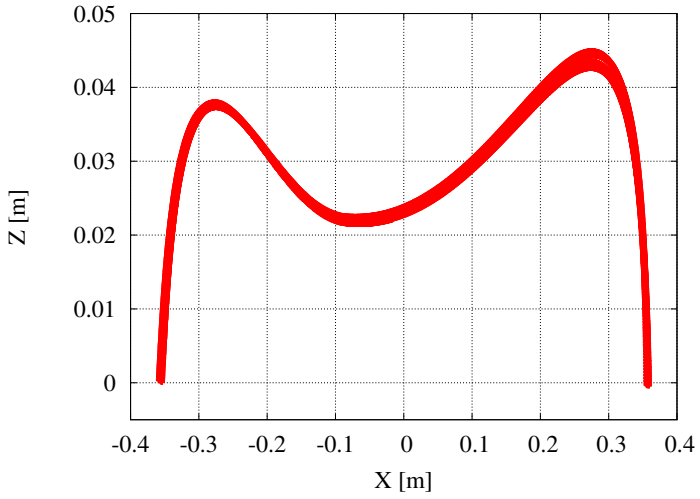

(b)

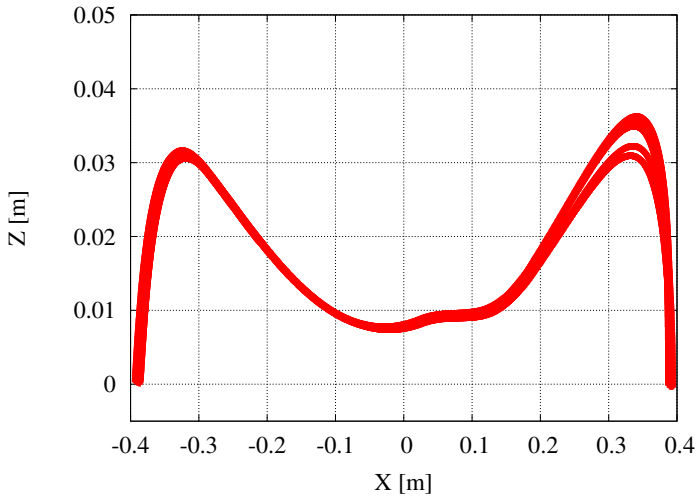

(c)

Fig. B.1: Comparison of foot-clearance: (a) Trajectory of the foot of the swing leg without active knee-lock, (b) Trajectory of the foot of the swing leg with the motion in the frontal plane, (c) Trajectory of the foot of the swing leg with active knee-lock.